

ON QUALITY REQUIREMENTS TO THE BARIUM FLUORIDE CRYSTALS

January 3, 1992

Ren-yuan Zhu
California Institute of Technology

Abstract:

Barium fluoride (BaF_2) crystal calorimeter is one of two options being pursued by the GEM collaborating as a candidate precision electromagnetic calorimeter. This report summarizes the considerations on quality requirements to the BaF_2 crystals.

ON QUALITY REQUIREMENTS TO THE BARIUM FLUORIDE CRYSTALS

Ren-yuan Zhu

Lauritsen Laboratory
California Institute of Technology
Pasadena, CA 91125

January 3, 1992

Abstract

Barium fluoride (BaF_2) crystal calorimeter is one of two options being pursued by the GEM collaborating as a candidate precision electromagnetic calorimeter. This report summarises the considerations on quality requirements to the BaF_2 crystals.

1 INTRODUCTION

Total absorption shower counters made of inorganic scintillating crystals have been known for decades for their superb energy resolution and detection efficiency. In high energy physics, large arrays of such counters have been assembled for the detection of photons and electrons at e^+e^- storage rings. A recent example is an electromagnetic calorimeter consisting of 12,000 large size BGO crystals constructed for the L3 experiment at LEP [1]. Because of its unique physics capability, crystal calorimeter has also attracted much attention in high energy physics community proposing experiments for next generation accelerators: Superconducting Super Collider (SSC) at U.S. and Large Hadronic Collider (LHC) at Europe.

Much progress has been made towards the choice of material, and production of large size crystals for SSC and LHC, where high speed and superb radiation resistance are primary requirements. Attention is now concentrated on three fluoride crystals: barium fluoride (BaF_2) [2], cerium fluoride (CeF_3) and lead fluoride (PbF_3) [3].

The BaF₂ calorimeter is one of two principal options for electromagnetic calorimetry in the “Gammas, Electrons and Muons” (GEM) experiment [4], which is one of the two major general-purpose detectors proposed for the SSC experimental program. To maximize its discovery potential, the GEM detector has been designed to be a precision lepton and photon detector. A precision electromagnetic calorimeter, as well as a high resolution muon system, are the two principal ingredients of the GEM detector design.

This report concentrates on expected performance of BaF₂ electromagnetic calorimeter at the SSC, and corresponding requirements to the quality of BaF₂ crystals to be used in constructing calorimeter. Section 2 of this report gives a brief description of the concept of BaF₂ calorimeter design. The performance of the BaF₂ calorimeter is illustrated in section 3. The systematic effect on energy resolution from light response uniformity and radiation resistance are deliberated in sections 4 and 5. The inter-calibration accuracy and specifications for BaF₂ crystals are discussed in section 6 and 7.

2 BaF₂ CALORIMETER DESIGN

Barium Fluoride (BaF₂) is a unique high density inorganic scintillator with three emission spectra peaking at 195 nm, 220 nm and 310 nm, with decay time constants of 0.87, 0.88 and 600 nsec respectively [5]. The intensity of the fast components have no temperature dependence — which should give a BaF₂ calorimeter greater intrinsic stability than the L3 BGO calorimeter — while the slow component increases with decreasing temperature at a rate of -2.4%/°C [6]. The speed of the fast components enable the detector to be gated in a single beam crossing at the SSC. Table 1 lists the basic properties of barium fluoride, as compared to other commonly used scintillation crystals: NaI(Tl), pure CsI, CsI(Tl), CeF₃ and BGO.

2.1 Design

Figure 1 shows the conceptual design of the BaF₂ calorimeter, which consists of two parts:

Table 1: Properties of Scintillation Crystals.

	NaI(Tl)	Pure CsI	CsI(Tl)	BaF ₂	CeF ₃	BGO
Density(g/cm ³)	3.67	4.51	4.51	4.88	6.16	7.13
Radiation Length (cm)	2.59	1.85	1.85	2.06	1.68	1.12
Moliere Radius (cm)	4.8	3.5	3.5	3.39	2.63	2.33
Interaction Length (cm)	41.4	37.0	37.0	29.9	26.2	21.8
X_{rad}/X_{int}	0.063	0.051	0.051	0.068	0.065	0.051
Refractive Index	1.85	1.80	1.80	1.49	1.62	2.15
Hygroscopic	Yes	No	No	No	No	No
Luminescence(nm)	410	300	565	310	340	480
(Peak Wavelength)				210	300	
Decay Time(nsec)	230	10	900	630	20	300
Light Output	100	20	45	0.9 20 4	5 6 ?	15

- A central barrel calorimeter with an inner radius of 75 cm and an outer radius of 140 cm, covering a rapidity range of $|\eta| \leq 1.32$ ($30^\circ \leq \theta \leq 150^\circ$).
- Two endcaps, located at $z = \pm 164$ cm, covering a rapidity range of $1.32 \leq |\eta| \leq 2.5$ ($9.4^\circ \leq \theta \leq 30^\circ$ and $150^\circ \leq \theta \leq 170.6^\circ$).

The total crystal volume of the BaF₂ calorimeter is 10.6 m³, with a total crystal weight of 51.8 t. Table 2 shows the basic parameters of the BaF₂ calorimeter.

The fine granularity ($\Delta\eta \approx \Delta\phi \approx 0.04$) and hermetic design of BaF₂ calorimeter provides a uniform response over the phase space coverage and a small 2.7% dead space for the cable path of central tracker. In summary, the BaF₂ calorimeter has the following features which are deliberated in the next section.

- **Time Resolution:** gating time in less than 16 ns (a single beam crossing);
- **Position Resolution:** δx and $\delta y \approx 1$ mm at the front surface of crystals;
- **Energy Resolution:** $(2.0/\sqrt{E} \oplus 0.5)\%$;

Table 2: Features of the BaF₂ Calorimeter

Detector	Barrel	Two Endcaps
Rapidity Coverage	$ \eta \leq 1.32$	$1.32 \leq \eta \leq 2.5$
Crystal Front/Rear Face (cm ²)	3.1 × 3.1 / 5.2 × 5.2	2.3 × 2.3 / 3.1 × 3.1
Crystal Length (cm)	50	50
Crystal Number	10,880	4144
Crystal Volume (m ³)	8.4	2.2
Crystal Weight (t)	41.1	10.7

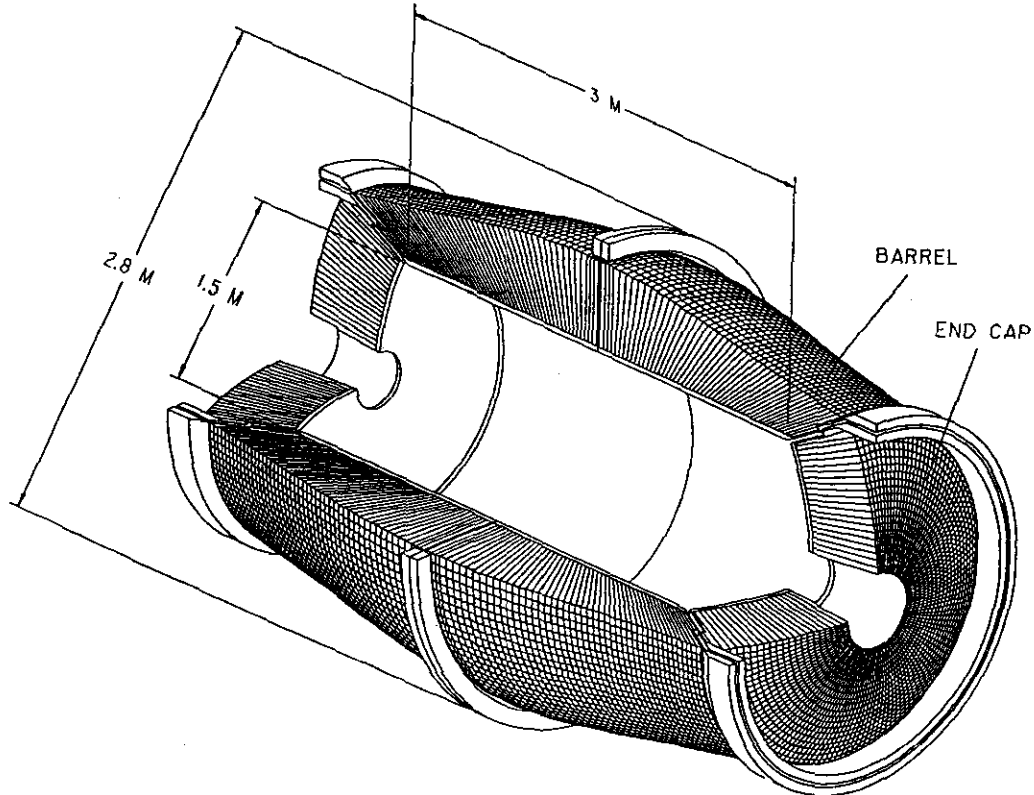


Figure 1: Conceptual view of the BaF₂ EM calorimeter.

3 BaF₂ CALORIMETER PERFORMANCE

3.1 Time Resolution

The intrinsic intensity of the slow scintillation component (600 nsec) in BaF₂ is 5 times higher than the fast components. Although the slow component may be

suppressed in a relatively straightforward way by sampling the output of each channel just before, and a few fast-decay-time constants after the start of a pulse [7], the intrinsic slow component could limit the dynamic range of photosensitive device, and could lead to pileup noise that could degrade the energy resolution.

Direct approaches for suppressing the slow component have been pursued over the last three years. An intrinsic suppression was discovered by Schotanus *et al.* [8]. They found that a small amount of lanthanum added to the crystal during growth greatly suppressed the slow component without significantly affecting the fast component. A subsequent study by Woody *et al.* [9] showed that there are several dopants which produce strong slow component suppression and retain high fast component light output. However, only lanthanum still preserves the radiation hardness of the pure material up to a level beyond 10^6 Rads.

Figure 2 shows the emission spectra for pure BaF_2 and BaF_2 doped with 1% of lanthanum. The peak intensity of the slow component (310 nm) is reduced by a factor of about five with little change to the fast components (195 and 220 nm).

Since the manufacture of large undoped high quality BaF_2 crystals is inherently

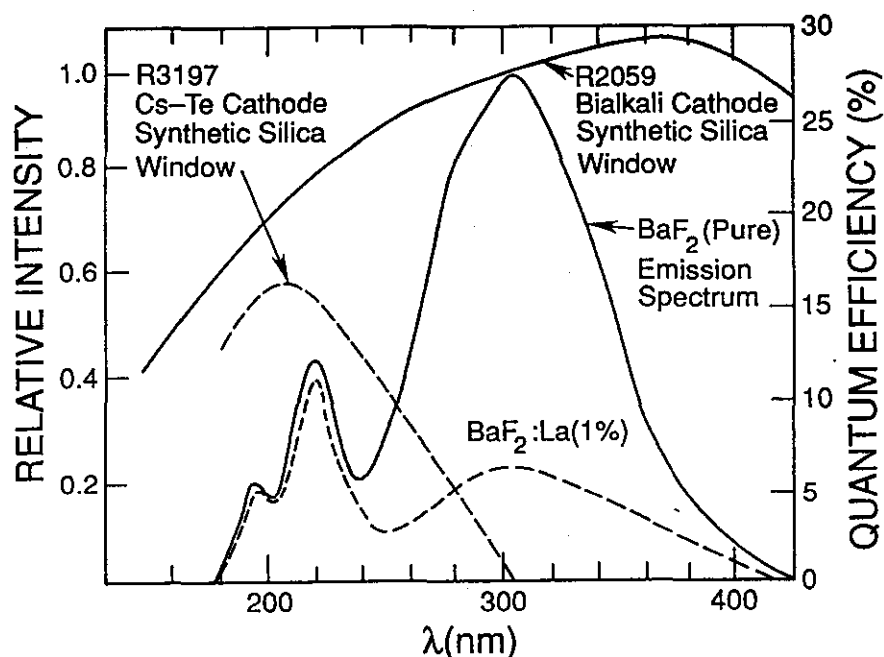


Figure 2: BaF_2 scintillation spectra and PMT quantum efficiencies.

simpler, and since the fast and slow scintillation components of BaF_2 peak at different wavelengths, a UV-selective photodevice (optimised for maximum sensitivity in the 220 nm region) is proposed to partially suppress the slow component. The slow component suppression is completed by a fast shaper, and by readout samples just before and shortly after the peak of the pulse. This technique of selecting the fast component does not restrict the dynamic range, and it allows us to maintain very low noise because of the low capacitance of the vacuum photodevice.

Figure 2 also shows the spectral sensitivity of a UV-selective 'solar-blind' photomultiplier (PMT) with a Cesium Telluride (Cs-Te) photocathode (Hamamatsu R3197) and a PMT with a bialkali photocathode (Hamamatsu R2059). Both PMT's have a synthetic silica (quartz) windows. The Cs-Te photocathode has a quantum efficiency of 10% around 220 nm, while the bialkali photocathode has a quantum efficiency of about 18% around 220 nm. It is clear that the solar-blind photocathode (Cs-Te) is mainly sensitive to the fast scintillation light.

An additional optical suppression of the slow component recently has been achieved by using new photocathodes, K-Cs-Te or Rb-Te, developed by Hamamatsu [10]. Both cathodes have about 10% quantum efficiency at 220 nm and provide better suppression of the slow component (by around a factor of 2 relative to Cs-Te). Figure 3 shows pictures of the scintillation light pulses recorded on an HP54111D digital scope using a bialkali photocathode (a and e), a Cs-Te photocathode (b and f), K-Cs-Te cathode (c and g) and a Rb-Te cathode (d and h). The rise time of the scintillation light pulse in these pictures was completely dominated by the 2.3 nsec rise time of the PMT's. On an expanded scale (a, b, c and d) the full width at half maximum of the fast scintillation light is measured to be 4—6 nsec. The optical suppression factors (F/S) for the slow component, defined as the number of photoelectrons in the fast components (F) divided by the number of photoelectrons in the slow component (S), are also shown in the figure.

An existing photodevice, R4406, may be used in BaF_2 readout. It has quartz window and K-Cs-Te cathode. The triode also has a gain of more than 50% of its nominal value when operating in a 1 tesla magnetic field with an angle of 45° or less to its axis [11]. Note, the synthetic silica (quartz) window has very high radiation resistance against photon and neutron doses [12]. Another choice of photodevice is proximity focused 5 stage phototube, recently proposed by Hamamatsu [13], which

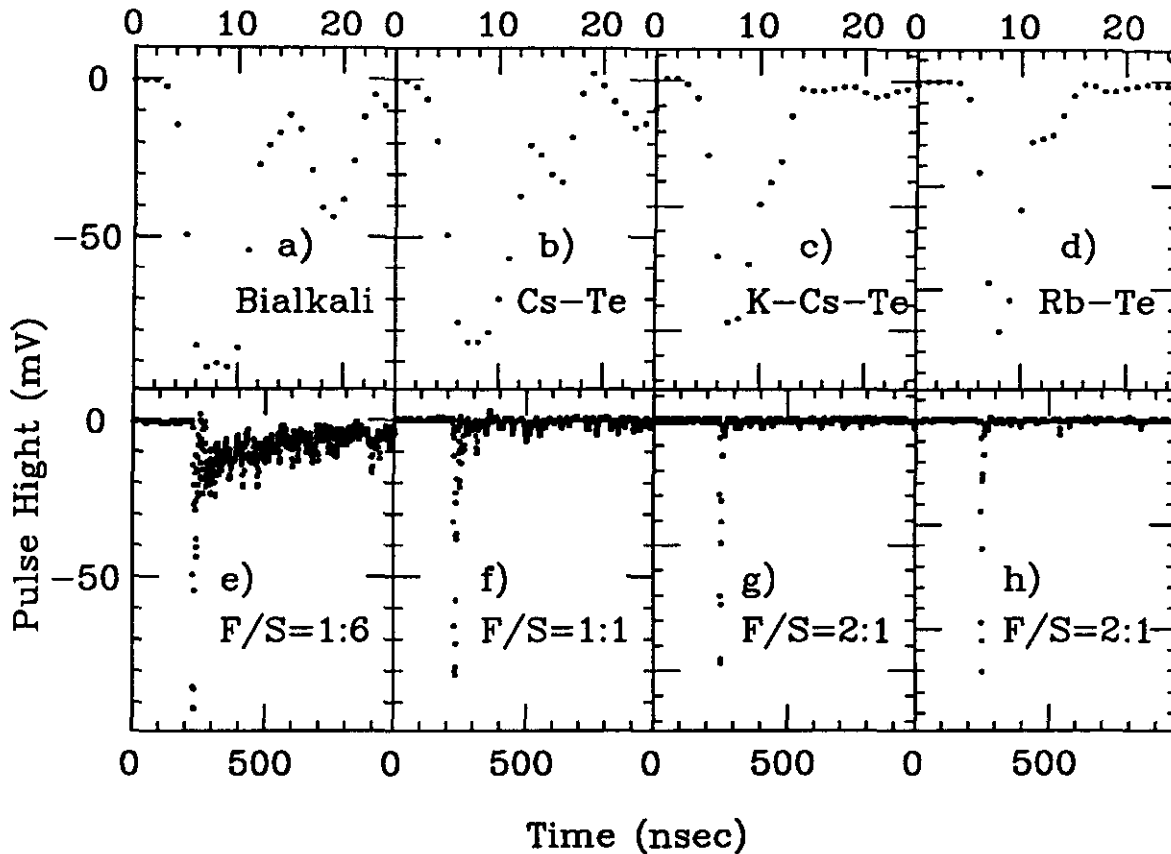


Figure 3: BaF_2 scintillation Light pulse observed by a bi-alkali cathode (a and e), a Cs-Te cathode (b and f), a K-Cs-Te cathode (c and g), and a Rb-Te cathode (d and h).

has gain of >30 under .8 tesla magnetic field.

3.2 Position Resolution

The position of an electromagnetic shower without longitudinal sampling, i.e. the coordinate of the impact point of an electron or a photon on the front surface of an electromagnetic calorimeter, is usually measured by using the center of gravity method. The position resolution of a calorimeter thus depends on its structure, especially the lateral cell size. For a calorimeter organized in pointing towers, the

position resolution as a function of energy can be parametrized as:

$$\delta x \text{ (mm)} = \frac{3}{\sqrt{E}} e^{0.4D} \quad (1)$$

where E is the energy of the particle being measured in GeV, and D is the cell size in radiation lengths.

A proper lateral cell dimension thus is very important. Its choice is usually a compromise between good position resolution, shower containment in a 'tower' consisting of a moderate number of lateral cells, and the total number of readout channels (which is reflected in the cost). Good position resolution as well as a good knowledge of the transverse shower shape (important for e/π resolution) favour a small cell size, while shower containment in a few cells favors a larger size. A cell dimension in the neighborhood of approximately one Moliere radius is usually taken, corresponding to $\approx 75\%$ of shower energy deposited in the center cell.

All of these factors taken together have led to a technical consensus that the optimum lateral segmentation is $\approx 0.04 \times 0.04$ ($\Delta\eta \times \Delta\phi$) at the SSC as in the BaF₂ design. This segmentation results a position resolution, calculated according to Eq. 1 for a 20 GeV electron or photon, is 1.2 mm, which is comparable with what has been measured with L3 BGO calorimeter [1].

3.3 Energy Resolution

The energy resolution of an electromagnetic calorimeter can be parametrized as:

$$\left(\frac{\delta E}{E}\right)^2 = \left(\frac{a_0}{E}\right)^2 + \left(\frac{a_1}{\sqrt{E}}\right)^2 + b^2 \quad (2)$$

The contributions of each term to the resolution are:

- a_0 is the contribution from electrical noise, summed over a few Moliere radii around the maximum of the lateral shower distribution;
- a_1 is the contribution from the photoelectron statistics;
- the systematic term b has three contributions:

$$b^2 = b_n^2 + b_G^2 + b_C^2 \quad (3)$$

- b_G represents the geometry effect, including shower leakage at the front, side and back of the detector and inactive material between cells;
- b_n represents physics noise, including fluctuations of the shower and uniformity of light response etc.;
- b_C represents intercalibration error.

At low energy, the dominant contribution to the energy resolution is the noise term (a_0), which decreases quickly with increasing energy. The sampling term (a_1) dominates in the range of medium to high energies until a high energy limit is reached, where the systematic term (b) dominant.

In this section, only systematic term b_G is discussed. The systematic terms of b_n (light response uniformity) and b_C (inter-calibration) are deliberated separately in sections 4 and 5.

3.3.1 Light Yield: a_1

It is not very difficult to build a homogeneous electromagnetic calorimeter with a small a_1 term. A photoelectron (p.e.) yield better than 10 p.e./MeV would be enough to provide an $a_1 = 1\%$. Figure 4 shows the measured ^{137}Cs spectra obtained from the same BaF_2 sample by using four PMTs with different photocathodes (bialkali, Cs-Te, K-Cs-Te and Rb-Te) for two different gate widths (55 ns and 2 μs). By comparing the spectra, it is clear that the K-Cs-Te cathode has good quantum efficiency (better than Cs-Te and Rb-Te) in detecting the fast components from BaF_2 . Measurements at Caltech show that more than 50 p.e./MeV are obtained from typical 25 cm long BaF_2 crystals by using K-Cs-Te photocathodes.

The light yield of 50 cm long crystals has been measured at Caltech with ^{137}Cs γ -ray source and at Fermi Lab with electron beam. For production quality BaF_2 crystals, photoelectron yield was measured to be 20 to 50 p.e./MeV by using K-Cs-Te or Rb-Te photocathode with good light response uniformity (see Section 4). This corresponds to an a_1 term of about 0.4—0.7%.

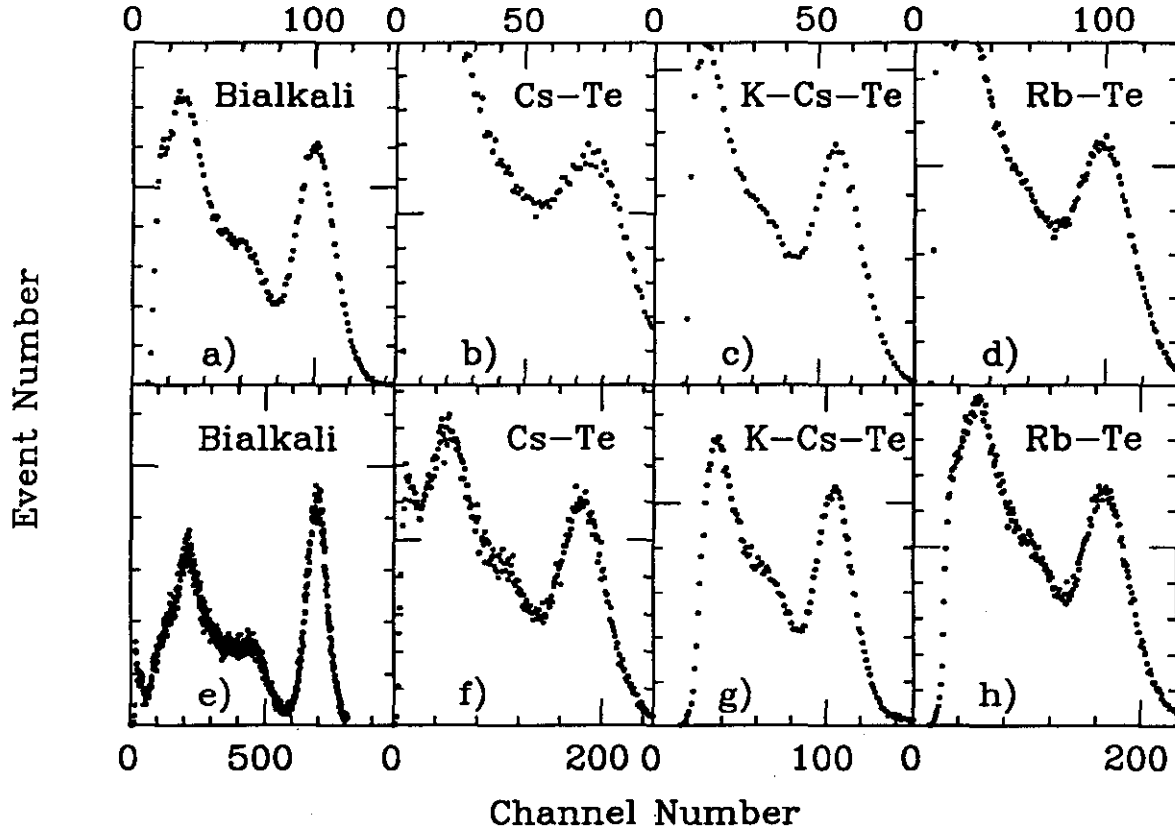


Figure 4: ^{137}Cs spectra measured with 4 PMTs with different photocathodes for two different gate widths: 55 ns (a–d) and 2 μs (e–h).

3.3.2 Electrical Noise: a_0

Because of its small capacitance (10 pf) and small dark current (0.1 nA), it is not difficult for the R4406 vacuum phototriode and the front electronics to provide an electrical noise level of 2,000 electrons per channel [14]. In reality, one needs to sum over a few Moliere radii to reconstruct an electromagnetic shower. In the case of using 3×3 crystals, which contains more than 95% of shower energy according to GEANT simulations [15], the intrinsic electrical noise is 6,000 electrons without channel-to-channel correlations. Assuming the minimum gain of the R4406 phototube is 6, i.e. 50% of its nominal gain of 12 in the worst magnetic field situation [16], the signal corresponds to 120,000–300,000 electrons/GeV with a K-Cs-Te photocathode. This means an a_0 term of 2–5% for 3×3 crystal readout, if existing R4406 is used. The a_0 term can be further reduced if the proximity focused

5 stage phototube [13] is used. Since it has a gain of >30 under .8 tesla magnetic field, the a_0 term can be further reduced to 0.4—1%. The electrical noise introduced by channel-to-channel correlations, however, must be reduced by carefully implementing the electrical isolation between the readout channels.

3.3.3 Geometry Effect: b_G

To reduce the systematic effects caused by shower leakage and inactive material, a precision electromagnetic calorimeter must be designed to contain nearly the complete electromagnetic shower, over the whole energy range. Since electromagnetic shower physics is well understood, a complete GEANT simulation would be able to predict the resolution of a calorimeter with proposed geometry configuration. To reduce the term b_G , an electromagnetic calorimeter must be designed with enough length and have minimum dead material in the front, between cells and, especially inside the calorimeter.

A detailed GEANT simulation was carried out to estimate the effect of shower leakage and non-active material for the BaF_2 design [17]. Figure 5 shows a prototype of BaF_2 matrix used in this simulation, which consists of 121 (11×11) BaF_2 crystals with the proposed size: $3 \times 3 \text{ cm}^2$ at the front, $5 \times 5 \text{ cm}^2$ at the back and 50 cm long. Effects included in the simulation are:

- 250 μm carbon fiber wall between crystals;
- shower leakage because of summing a limited number (3×3 or 5×5) of crystals; and
- 0.30 radiation lengths of aluminum, representing the beam pipe, tracker, and carbon fiber mechanical support, at the front of the BaF_2 array.

Particles were shoot uniformly at the front surface of the center crystals of the array. The energies deposited in each crystal, in the carbon fiber walls between crystals, in the aluminum and leaking out sideways were recorded. The result of this simulation for electrons with different energies (5, 10, 100 ad 500 GeV), in terms of σ of the peak, full width at half maximum (FWHM) divided by 2.35, is listed in Table 3.

A further study was carried to look the systematic effect of carbon fiber wall.

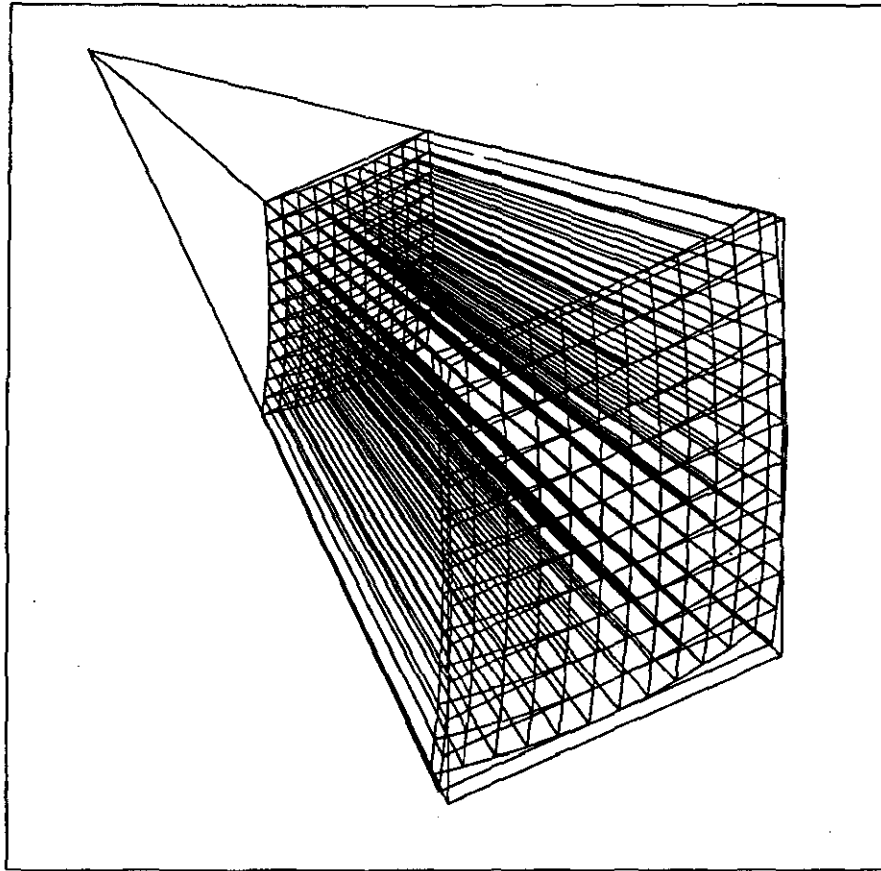


Figure 5: BaF₂ prototype used in simulation.

By varying the thickness of carbon fiber walls from 0 to 250 μm , the resolution obtained showed no observable difference [17]. This indicates that the systematic effect of support structure is negligible.

Table 3: Energy Resolution (%)

E (GeV)	5	10	100	500
Electrical Noise	0.4	0.2	0.02	0.004
Photoelectrons	0.2	0.14	0.045	0.02
GEANT	0.60	0.43	0.31	0.29
Intercalibration	0.40	0.40	0.40	0.40
Total	0.85	0.63	0.51	0.49

3.3.4 Summary of the Energy Resolution

Table 3 summarizes the BaF_2 resolution, including the contributions from electrical noise, photoelectron statistics, intrinsic resolution from GEANT simulation and the intercalibration. Based upon the discussion in section 6, a precision of intercalibration of 0.4% is assumed. Note, in this simulation the light response uniformity was assumed to be under control. The real effect of light response uniformity is discussed in section 4. The result of the energy resolution is shown in Fig. 6b. It can be parametrized as $2\%/\sqrt{E} \oplus 0.5\%$, which is also shown in Fig. 6b as a solid line.

As a comparison, Fig. 6a shows the energy resolution measured with 4000 BGO crystals (half barrel) in a CERN test beam [1]. In the energy range beyond 20 GeV, the dominant contribution to the energy resolution is the systematic intercalibration uncertainties. The resolution of the L3 BGO calorimeter may also be parametrized as $2\%/\sqrt{E} \oplus 0.5\%$, which is also shown in the Fig. 6a as a solid line.

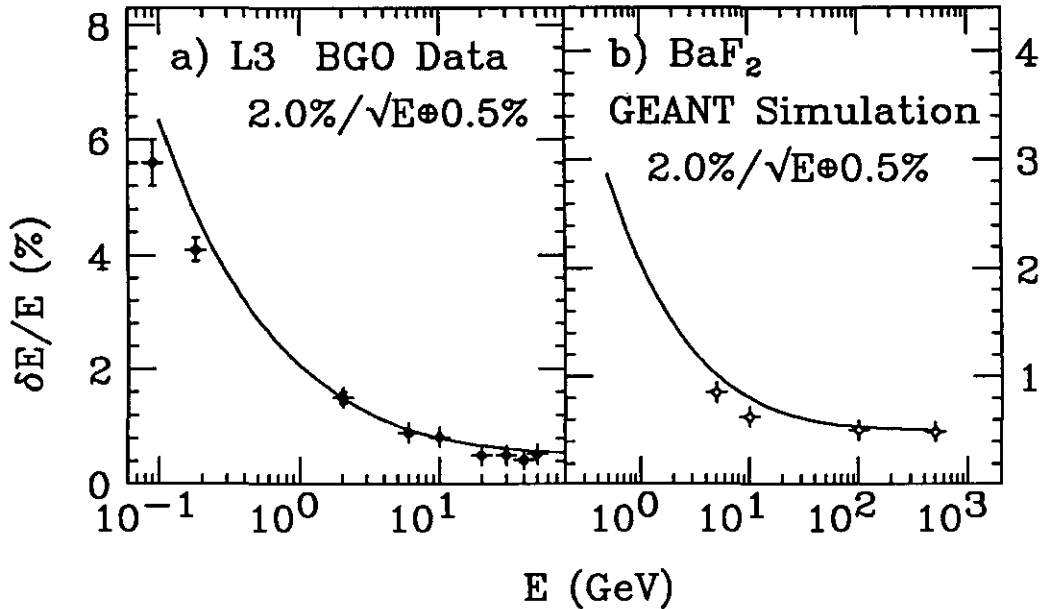


Figure 6: Energy Resolution of L3 BGO calorimeter (a), measured at CERN test beams with 4000 crystals, and BaF_2 calorimeter (b), calculated with GEANT simulation. The solid curves represent a simple parametrization of $2\%/\sqrt{E} \oplus 0.5\%$.

4 LIGHT RESPONSE UNIFORMITY: b_n

Experience with the L3 BGO, and other precision crystal calorimeters, has shown that light response uniformity at the level of several percent over the length of the crystal (except for the first few and the last few radiation lengths), is important to maintain the resolution. This uniformity is also needed to maintain good linearity over a large dynamic range, e.g. from ~ 10 GeV up to the TeV range at the SSC.

4.1 Effect of Light Response Uniformity

The consequence of light response uniformity has been studied with a GEANT simulation [17] (as described in section 3.3.3), assuming the effect of non-uniform light responses can be parametrized as a normalized function :

$$Y = Y_{25} [1 + \delta(Z/25 - 1)] \quad (4)$$

where Y_{25} represents the light yield at the middle (25 cm) of a BaF_2 crystal, δ represents the uniformity of the light response of a BaF_2 crystal, and Z is the distance from the small end of the crystal.

The effect of δ values of 5%, 10%, 15%, and 20% has been simulated. Fig. 7 shows the result of the simulation for sum of 3×3 crystals. As seen from Fig. 7, the response of energy deposition decreases when δ increases, while the energy resolution degrades. It is clear from the figure that it is vital to maintain the light uniformity within 5%.

4.2 Light Response Uniformity of 25 cm Long Crystals

The light response uniformity of BaF_2 crystals can be achieved by using special wrapping or coating method. For a tapered crystal with its 6 faces polished, there are two complementary factors which affect the light uniformity along the crystal axis: the attenuation and the optical focusing. While the first factor causes a decrease of the response with the increase of the distance to the light-sensitive device, the second factor causes an increase of the response. For a BGO crystal, the second factor dominates: a strong increase of light response to the small end

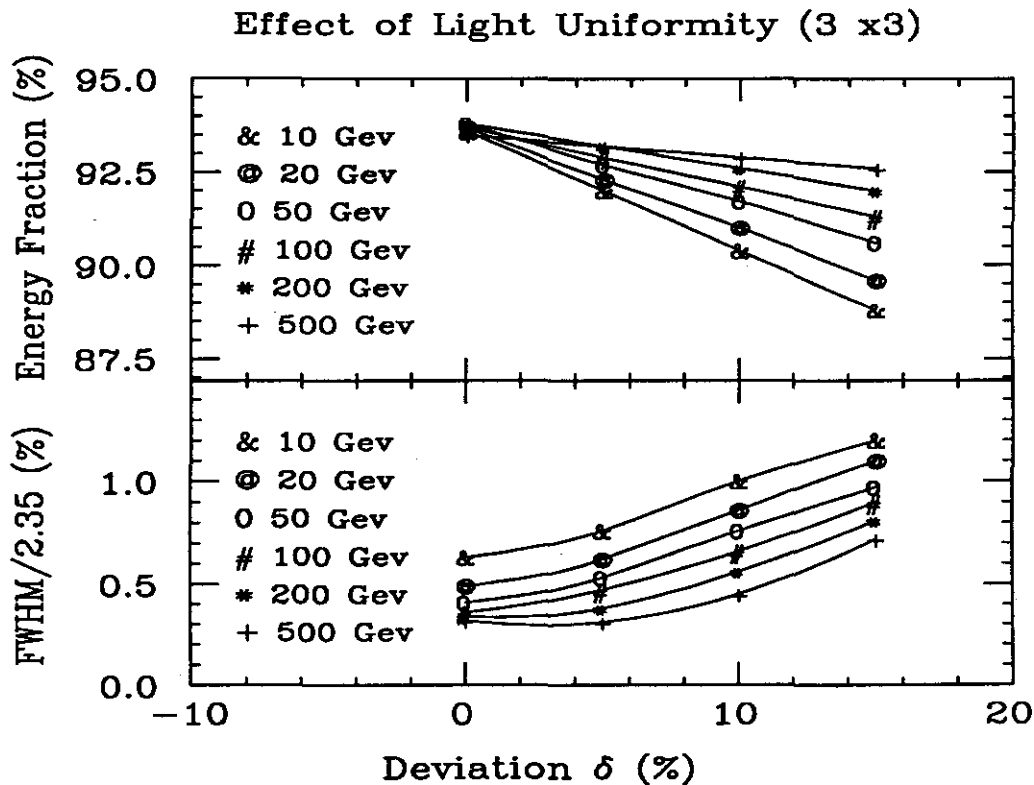


Figure 7: Effect of light uniformity predicted with GEANT simulation.

was observed for the L3 crystals [1]. Only after extensive studies of controlled depolishing of the surface, was light uniformity and high light collection efficiency achieved by coating the polished BGO crystals with a 40 to 50 μm thick layer of high reflective NE560 paint.

Figure 8a shows the light uniformity curves with and without the NE560 coating, measured with a ^{137}Cs source. The parameter R in Fig. 8a is the relative light output difference for the source at 21 cm and 3 cm from the photodiode. The crosses correspond to aluminized mylar wrapping and the diamonds to NE560 coating.

The optical focusing effect, however, is less important for the BaF_2 because of its smaller refractive index. The light collection uniformity of a 25 cm long BaF_2 crystal measured with a collimated ^{137}Cs source is shown in Fig. 8b. The photodetector used in this measurement is a photomultiplier (PMT) with a Cs-Te solar-blind photocathode (Hamamatsu R3197). With simple aluminum wrapping, the

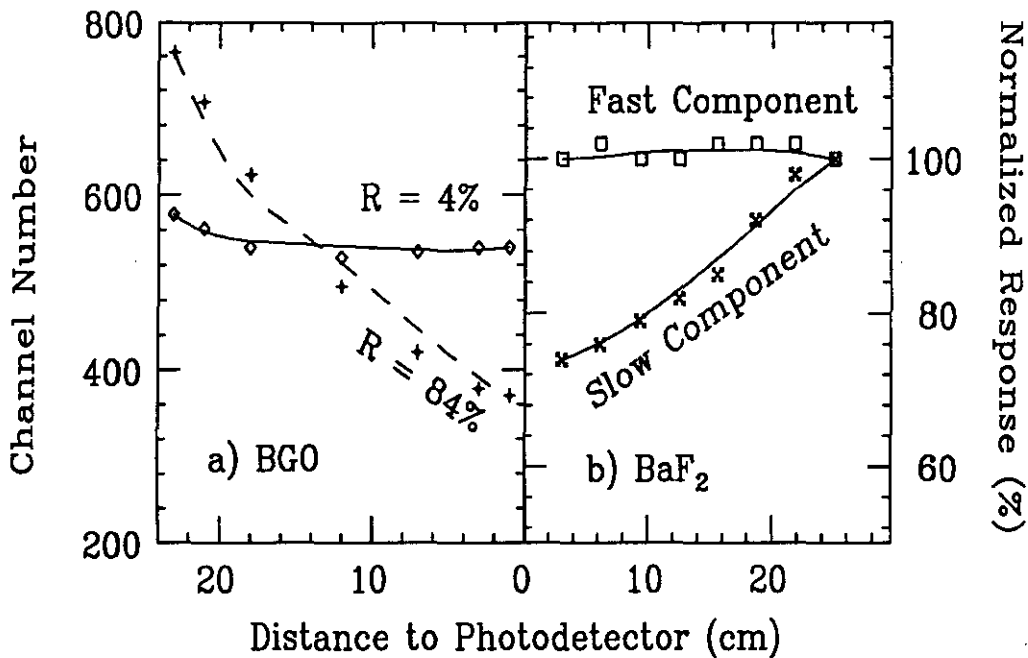


Figure 8: The light collection responses of L3 BGO crystals (a) and BaF₂ crystals (b), measured with a collimated ¹³⁷Cs source running along the axis of the crystals.

measured response of the fast scintillation component shows a uniformity within ~2% in a 25 cm crystal piece. Because of a longer light attenuation length, the response of the slow scintillation component shows an increase with an increasing distance from the PMT, as shown in Fig. 8b.

4.3 Light Response Uniformity of 50 cm Long Crystals

In order to extend the light uniformity results of 25 cm long crystals to the 50 cm long crystal-pairs which make up the prototype BaF₂ detector, two important technical difficulties must be overcome:

1. Find a glue with good UV transmission down to at least 200 nm. This is needed to optically couple the two crystal pieces together, as well as to couple the crystal-pair to the photodevice.
2. A technique of crystal surface treating: wrapping, or UV-reflective coating, to combine good light collection efficiency with overall uniformity.

4.3.1 KE103 Glue

While the best UV-transmitting optical coupling material (down to 190 nm) is Dow Corning 200 Silicone fluid, the best viscous grease, which can be used for good long-term joints if set up and used with care, is GE Silicone based UISC 600M. Although grease of this type have been used successfully on large BaF₂ crystals in experiments: by Woody at BNL, and by the TAPS Collaboration [20], there is no doubt that a glue is more secure.

Recent measurements by Kobayashi *et al.* at KEK [18] indicated that KE103 (an RTV glue) [19] is a candidate of UV transparent glue. Note, KE103 was also measured to be radiation hard up to a level beyond 10⁷ Rads [18]. The transmission results were measured at Caltech with hard-cured samples of KE103, as summarized in Table 4 below. Thin joints of KE103 were made by pressing two pieces of quartz together (typically few tens μm), and the UV transmittance was measured, normalized to the results obtained with Dow Corning 200 fluid between two similar pieces of quartz. The results for the GE grease UISC 600M are shown for comparison. As shown in the table, the transmission of KE103 adhesive is nearly as good as the Dow Corning fluid down to 200-205 nm, and it shows good transmission down to 190 nm.

Table 4: UV transmission (%) relative to Dow Corning 200 fluid, for thin layers of KE103 RTV and GE UISC 600M grease

Wavelength (nm)	190	195	200	205	210	215	220	225	230
KE103/1	97.2	87.6	90.5	94.6	97.8	98.3	99.9	99.4	99.4
KE103/2	83.7	88.5	95.3	97.6	98.8	99.8	99.4	99.9	99.8
UISC 600M		90.0	94.4	96.4	96.2	97.5	97.3	97.5	97.7

However, it should be pointed out that if the layer of KE103 glue is too thick, e.g. 500 μm , the joint is no longer transparent at UV. Figure 9 shows the transmittance measured for 500 μm thick layers of various adhesives. The cut-off at 220 nm of KE103 shows clearly that a bad joint of crystal pair would destroy light response uniformity.

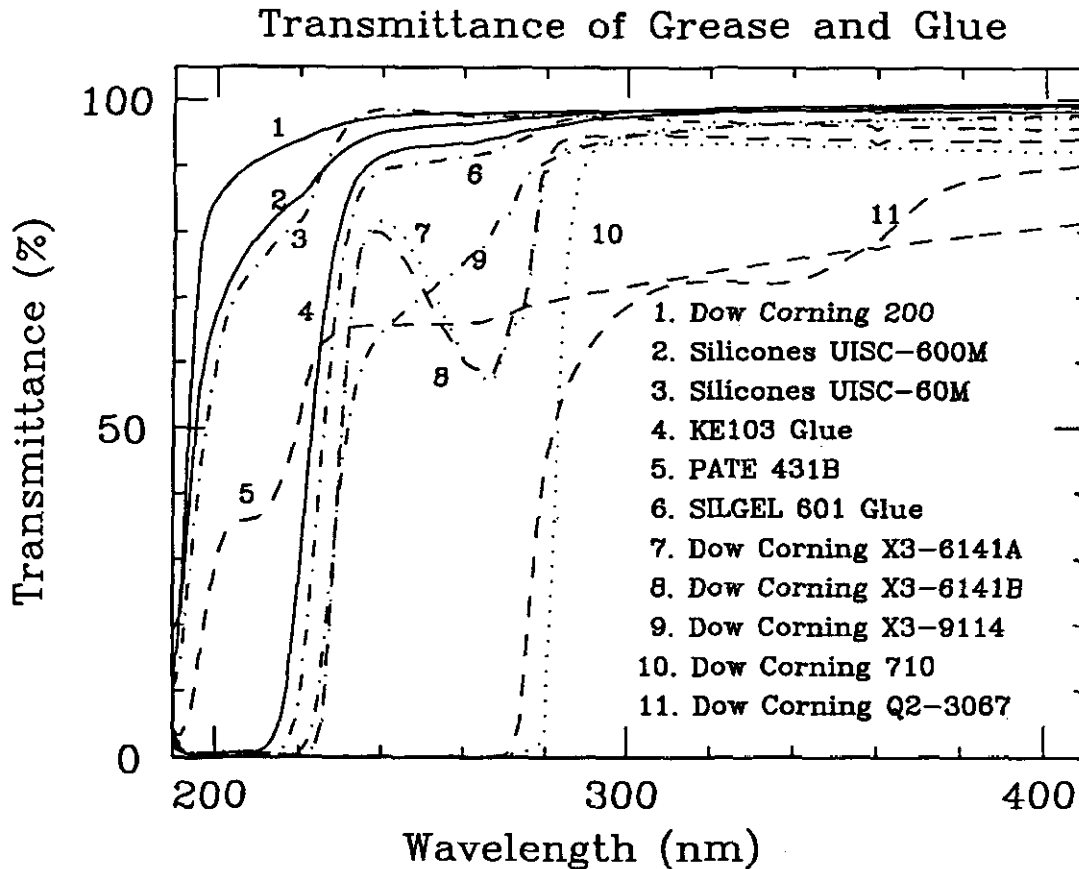


Figure 9: The Transmittance of 500 μm thick layers of various grease and glues.

4.3.2 Crystal Surface Treating

A simple wrapping technique, in which the region near the phototube is covered with black paper to suppress direct light was used for 49 test crystals. Similar techniques have been used to obtain good light uniformity in BaF_2 crystals by B. Winstein *et al.* at Fermi Lab. By adjusting the wrapping, a uniformity at the level of $\approx 5\%$ or better over the length was obtained for 50 cm long BaF_2 crystals with good glue joint. A result measured at Fermi Lab with a muon beam hitting a 50 cm long BaF_2 crystal pair transversely is shown in Figure 10.

Note, good uniformities were obtained in spite of the fact that there were substantial variations in the light output of the first crystal batches produced in 1990. It is also known that aluminum foil in contact with air is not a high-efficiency reflector for 200 nm light.

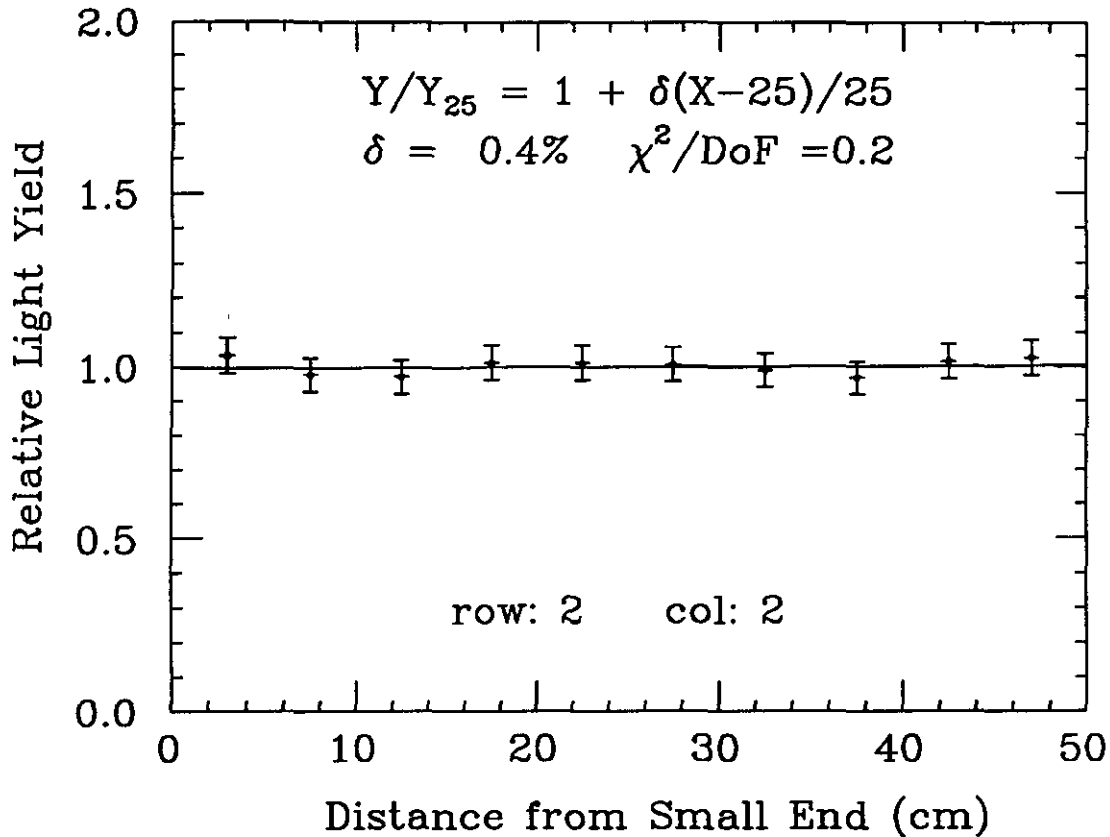


Figure 10: Normalised pulse height obtained with a 50 cm crystal pair measured with muon beam at Fermi Lab.

For the final BaF₂ system, one of the main R&D issues is investigation of a UV-reflecting coating, such as MgF₂ (used routinely for RICH Counter mirrors at 170 nm). The MgF₂ would be applied in a vacuum tank, immediately followed by a sealing layer of quartz. A masked pattern of reflector would be used to achieve the uniformity. This technique, which is not available during small-scale prototyping at moderate cost, would improve our light collection efficiency as well as the uniformity during mass production.

5 BaF₂ RADIATION RESISTANCE

All above discussions have not touched an important issue of BaF₂ calorimeter for the SSC: the radiation resistance. In this section we discuss the phenomena of

radiation damage of BaF₂ crystals. For more detailed discussions in this issue, see, for example, papers and talks presented in BaF₂ Workshop at Shanghai [21], May 1991, and in GEM BaF₂ panel meetings at SSCL [22,23], Beijing [24] and Shanghai [25], December 1991. Before discussing the radiation resistance, the production of BaF₂ crystals in China is addressed below.

5.1 Production of BaF₂ Crystals in China

The Shanghai Institute of Ceramics (SIC) is specialized in inorganic, non-metallic materials and materials science. The total work force of SIC consists of 200 professors, associate professors and senior engineers, 500 researchers and technicians and 300 skilled workers. SIC's research field includes synthetic crystals, advanced ceramics, special glasses and ceramic coatings, compositional analysis, structure analysis, instrumental design, and other related topics.

Studies of synthetic crystals started at SIC in 1960, including crystal growth, crystal physics, crystal chemistry and crystal devices. About 50 kinds of crystals have been studied so far, such as electro-optical crystals, acoustic-optical crystals, piezoelectric crystals and crystal scintillators. SIC has successfully studied the BGO crystals for L3, and established an R&D Center with a production capacity of 400 BGO crystals per month. By June 1990, 12,000 high-quality BGO crystals, meeting the specifications required for L3, were delivered to the L3 Collaboration.

Beijing Glass Research Institute (BGRI) has been working on synthetic crystal growth technology for many years. BaF₂ crystals were first developed at BGRI for infrared applications, and as crystal scintillators starting in 1985. During 1986-1988 BGRI and SIC collaborated on producing BaF₂ scintillators. By 1987, BGRI had grown a crystal 30 cm in length and 10 cm in diameter, using a modified Bridgeman method in vacuum. The technique has since been successfully adapted, at SIC as well as BGRI, to produce large BaF₂ crystal boules with the characteristic long truncated-pyramid shape required for GEM BaF₂ calorimeter, with a boule size up to 45 cm in length. Using these boules, BGRI has successfully produced crystal-pieces of 35 cm in length [26] after Shanghai Workshop.

In 1990, 49 pairs of BaF₂ crystals were delivered to Caltech for constructing a test matrix in Fermi Lab test beam. These crystals, ordered under generic

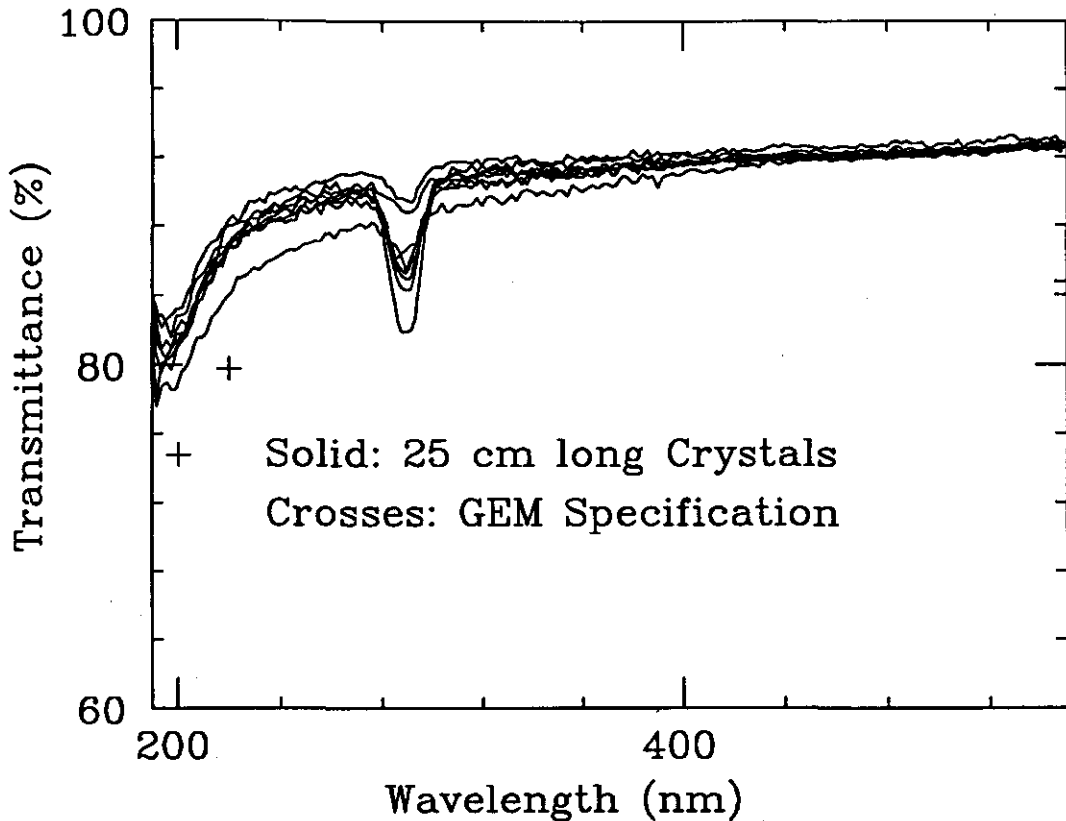


Figure 11: Optical transmission of 25 cm long crystals delivered by SIC and BGRI. The crosses represent the transmission specifications required by BaF₂ collaboration (see section 7).

R&D funding, have a reduced dimension ($2 \times 2 \text{ cm}^2$ instead of $3 \times 3 \text{ cm}^2$, at front) and do not meet radiation resistance requirement of SSC. Nevertheless, the transmittance of these crystals satisfies the specification proposed by BaF₂ collaboration. Figure 11 shows transmittance curves of several 25 cm long BaF₂ crystals from SIC and BGRI, together with the specifications shown as crosses. The details of specifications is discussed in section 7.

Using their own funds, SIC and BGRI have installed a total of ten crystal furnaces, which will bring the total production capacity to 90 crystal boules per month. The first computer-controlled mass production furnace with a production capacity of 40 crystals per month is now under construction in BGRI. It is expected that the crystal production capacity will be 130 boules per month, for which and associated R&D, SIC and BGRI have invested the equivalent of approximately \$

1.3M U.S. in hard currency. This does not include the labor costs for 28 full time persons at SIC, and 21 full time persons at BGRI.

5.2 Understanding BaF₂ Radiation Damage (I)

BaF₂ is one of the most radiation resistant crystal known. It is understood that the fast component in BaF₂ is produced by the “cross scintillation” mechanism [27]. Studies on other fluoride crystals have shown that this mechanism occurs in crystals with very high radiation resistance, and that it produces scintillation light with only a weak temperature dependence [27].

Early work done by S. Majewski and D. Anderson [28] showed that no color centers were formed in BaF₂ up to a dose of 1.3×10^7 Rads in an 800 GeV proton beam. The crystals tested were from Harshaw. Many other works [28] confirmed this early observation for irradiations from either charged particles or photons. It is also known that impurities in the crystal will cause radiation damage. An ab-

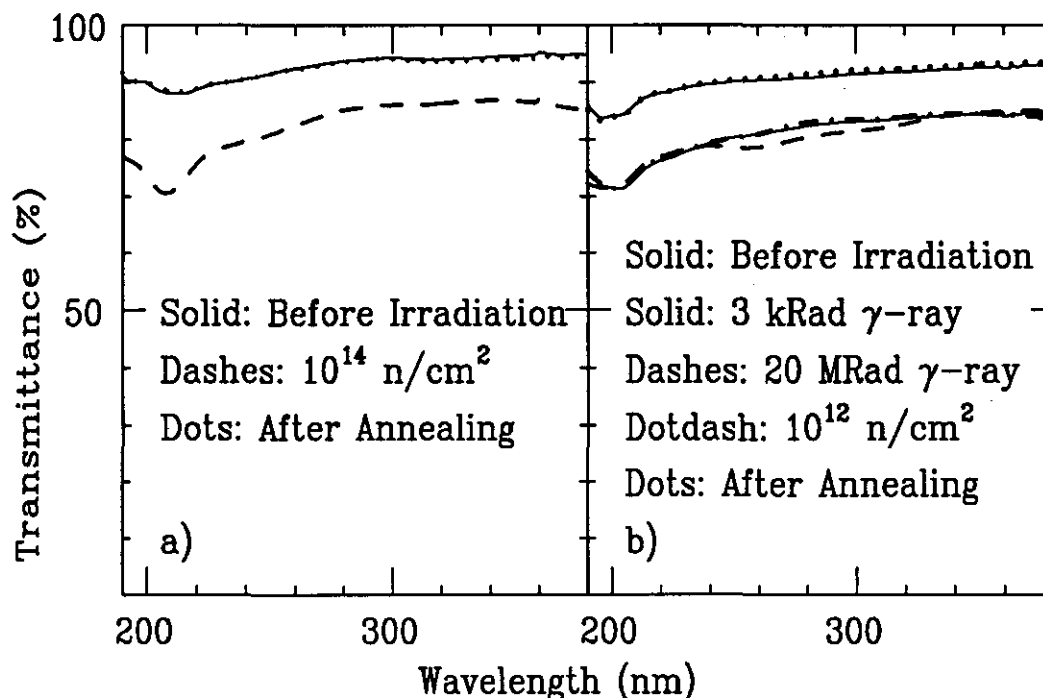


Figure 12: Transmittances before and after irradiation showing a) recovery from neutron damage; and b) typical saturation effect.

sorption band around 205 nm was identified as originating from Pb contamination [29], and this was correlated with the susceptibility to radiation damage.

Systematic studies of the radiation damage phenomena of BaF₂ have been performed. Tests show that the radiation damage of BaF₂ caused by either γ -ray or neutron irradiation is recoverable by annealing the crystal at 500°C for 3 hours [30]. Figure 12a shows the light transmittances before and after 10¹⁴ neutrons/cm² irradiation for a BaF₂ sample with 2.5 cm length. Also shown in the figure is the full recovery after annealing. This measurement indicates that neutrons, as well as photons, do not cause permanent damage to BaF₂ crystals.

BaF₂ crystals irradiated with γ -ray doses up to 20 MRads, and at the UC Irvine reactor with doses up to 10¹⁴ neutrons/cm², show that some initial damage occurs after the first 100 kRads, and no further damage follows (Fig. 12b). This saturation effect hints that the radiation damage in BaF₂ is not caused by an intrinsic color center in the bulk material of crystal, such as O²⁻ vacancies in BGO

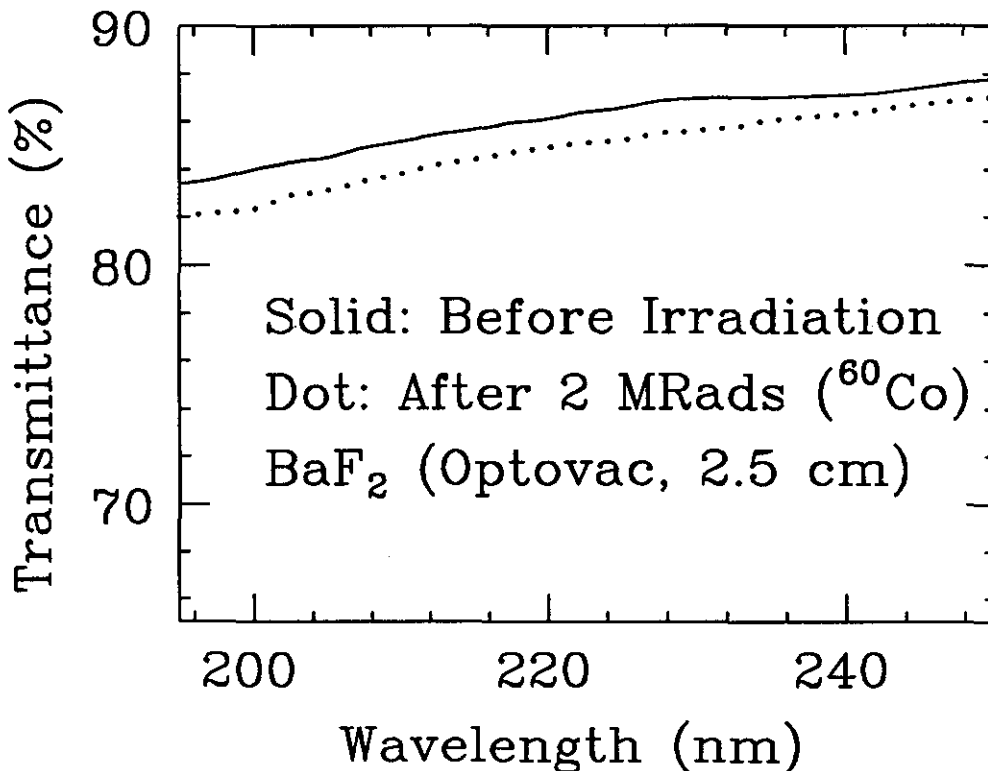


Figure 13: The transmittance of a 2.5 cm long BaF₂ crystal, as a function of wavelength, before and after 2 MRads dose measured by Woody *et al.*

[32], but by externally-introduced impurities.

The consequence of this initial damage has also been investigated. Figure 13 shows that the transmittance of a 2.5 cm long BaF₂ crystal decreased by ~1—2% after 2 MRad dose of ⁶⁰Co γ -rays [33]. This expected that a ~20% loss in transmittance for a 50 cm long crystal may be achieved for large size BaF₂ crystals with this quality.

Studies at Caltech, BNL, SIC and IHEP (Beijing) have also demonstrated that BaF₂ undergoes a striking recovery after a few hours' exposure to a UV lamp. The spectral component of the UV light in the 200 nm range required to break up the UV color-centers appears to be very low. A recent study by J.T. He (IHEP Beijing) for example, showed almost complete recovery after two hours' exposure to sunlight [31].

5.3 Radiation Resistance of 25 cm long Crystals

The first batch of 25 cm long BaF₂ crystals delivered in 1990, however, show substantial radiation damage, as measured at both BNL [22] and Caltech [23]. Figure 14 shows that the transmittance of 25 cm long crystals are reduced from 70—80% to 10—20 % at 220 nm for fast scintillation components of BaF₂ after 10,000 Rads of ⁶⁰Co γ -ray irradiation. The crystals tested are from SIC/BGRI and Merck. This situation was first extensively reviewed in May, 1991, in BaF₂ Workshop at Shanghai, and then in early December, in GEM BaF₂ panel meetings at SSCL, Beijing and Shanghai.

It is interesting, however, to note that there is almost no, spontaneous recovery of radiation damage around the wavelength of fast scintillation components of BaF₂ at room temperature. Figure 15 shows the transmittance spectra of the same two 25 cm long BaF₂ crystals from SIC/BGRI and Merck, before and 0 to 56 days after 1 MRads ⁶⁰Co γ -ray irradiation. The almost undistinguishable difference after 56 days of irradiation indicates that a stable detector may be made by BaF₂ crystals even with radiation damage. The key issue of a precision BaF₂ calorimeter thus is to control the damage before saturation.

Since May, 1991, substantial progress have been made at SIC and BGRI. Figure

16 shows that the transmittance of two 20 cm long crystals are reduced from 70—80% to 50—60% at 220 nm for fast scintillation components of BaF₂ after 1,000,000 Rads ⁶⁰Co γ -ray irradiation. The crystals are recently produced at SIC with improved processing technique. (Note, the figure shown was measured at Caltech, while the irradiation was done originally at SIC. A new figure will replace this one after our systematic measurements on these two new crystals by using JPL's radiation facility. It will be done by next GEM BaF₂ Panel meeting.)

According to chinese physicists (see section 5.5), they are confident in understanding the radiation damage mechanism of BaF₂ crystals, and in providing

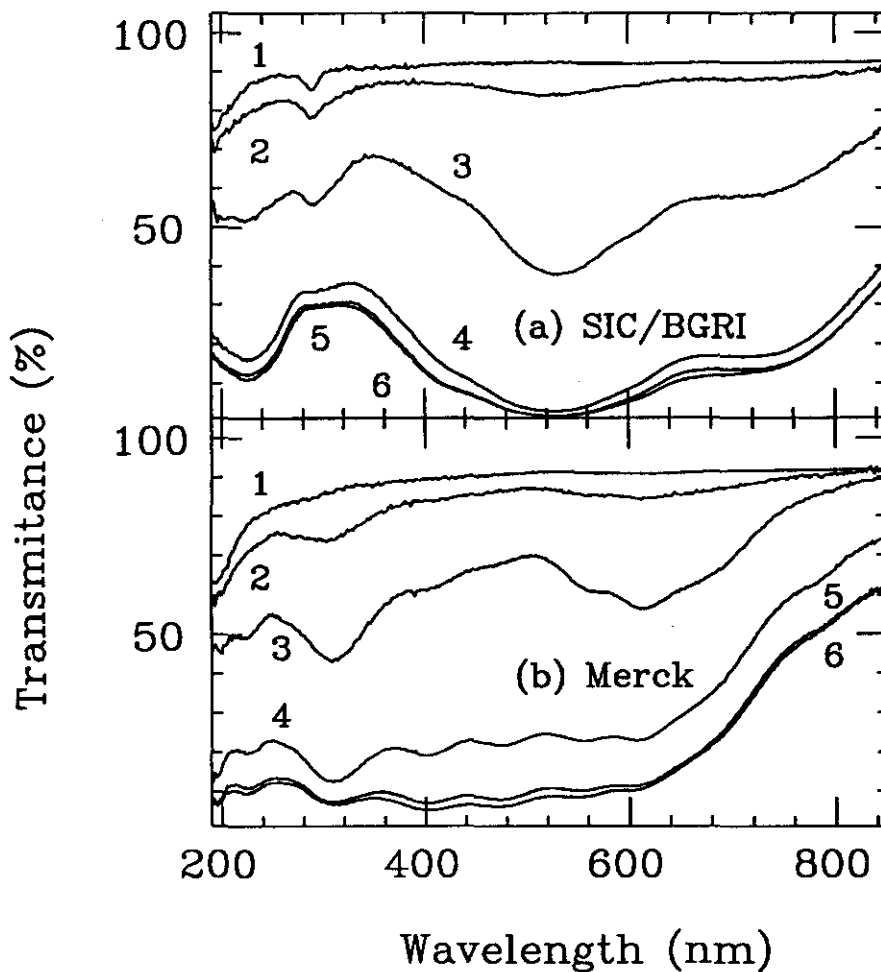


Figure 14: Transmittance spectra of 25 cm long BaF₂ crystals from SIC/BGRI (a) and Merck (b), before (1) and after ⁶⁰Co γ -ray irradiation with dosage of 100 (2), 1000 (3), 10,000 (4), 100,000 (5) and 1,000,000 Rads.

solutions for the problem. It is expected that 10% loss of transmittance may be achieved for 25 cm long crystals.

5.4 Consequences of Radiation Damage

There are three consequences in BaF_2 radiation damage:

1. radiation introduce color centers which cause absorption of scintillation light and thus reduce the light attenuation length;

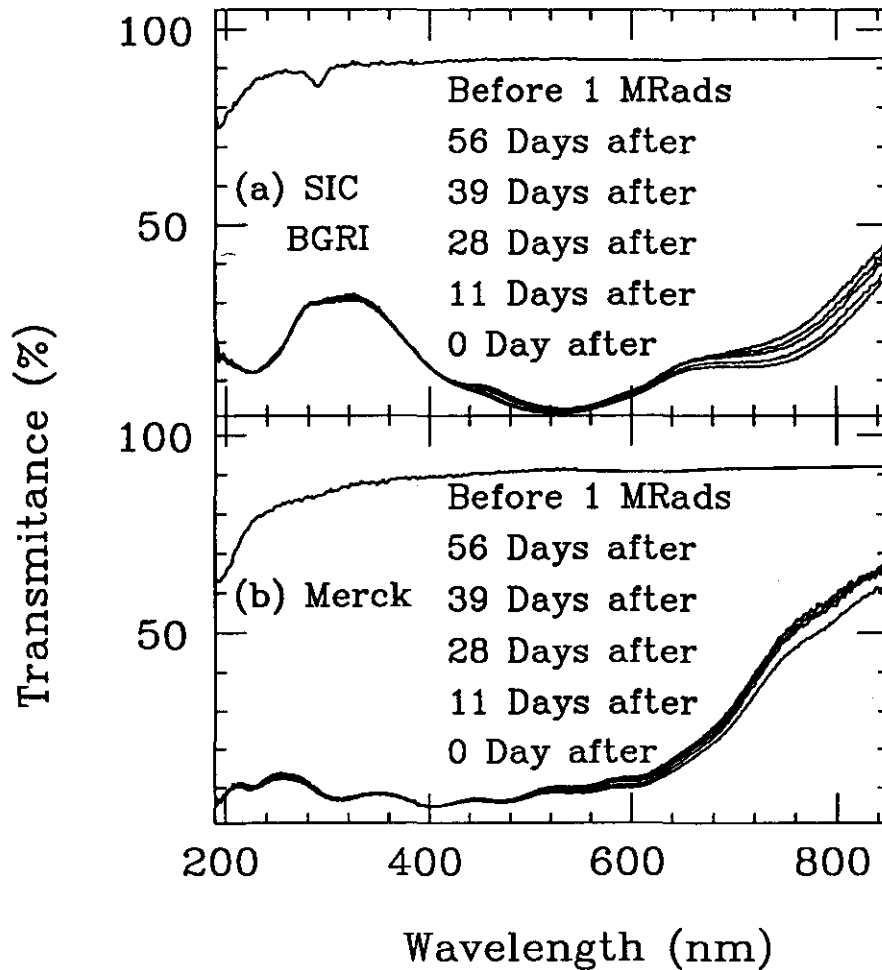


Figure 15: Transmittance spectra of a 25 cm long BaF_2 crystals before and after 1 MRads of ^{60}Co γ -ray irradiation. Also shown are spectra after 11, 28, 39 and 56 days after irradiation.

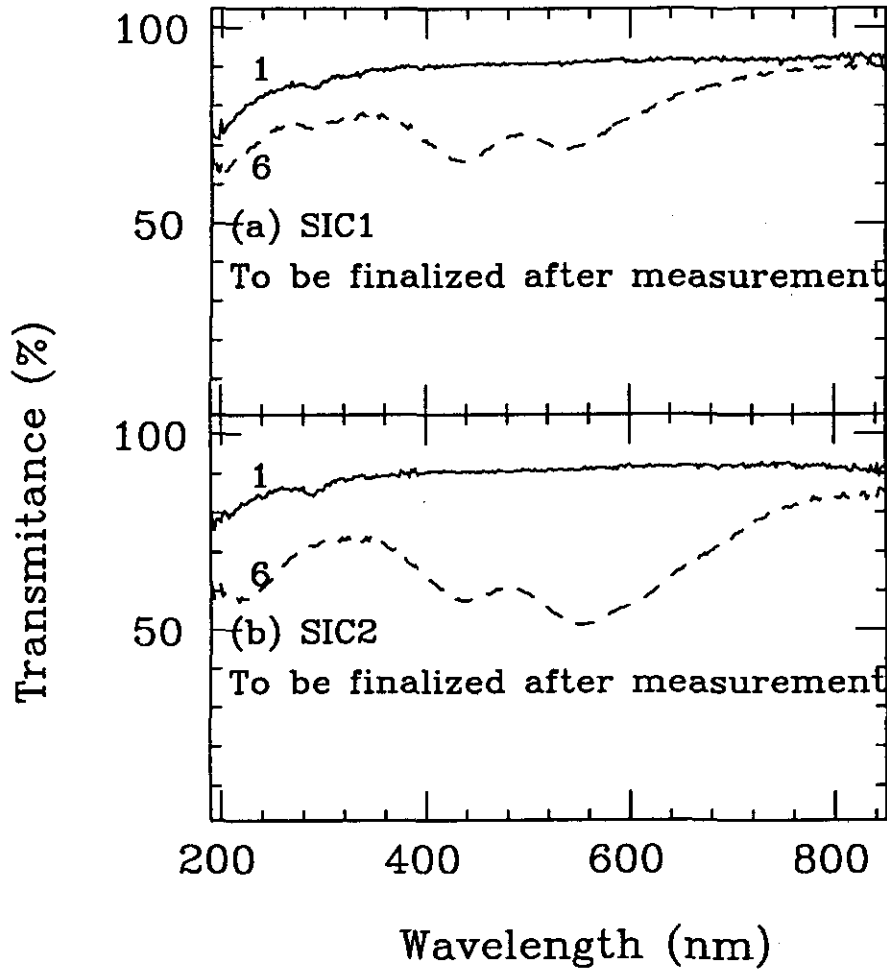


Figure 16: Transmittance spectra of 20 cm long BaF₂ crystals before (1) and after ⁶⁰Co γ -ray irradiation with dosage of 100 (2), 1000 (3), 10,000 (4), 100,000 (5) and 1,000,000 Rads.

2. radiation introduce phosphorescence which causes random background;
3. there might be a damage of the scintillation mechanism, and thus reduce the light yield.

Most early radiation damage studies were concentrated on the light absorption, i.e. the transmittance loss. Recent studies [22,34], however, reported observations of radiation introduced phosphorescence, which in many cases prohibits measurements of light yield of large size BaF₂ crystals with a conventional ¹³⁷Cs γ -ray source. Although causing inconvenience for laboratory study, the phosphorescence

can be treated as a random noise. Since its energy scale is very low, particularly since it is mainly in wave lengths longer than the fast components, we do not expect phosphorescence would degrade the precision of BaF₂ calorimeter.

It, however, is not clear if the radiation causes damage to the scintillation mechanism of BaF₂ crystals. Controversial results were reported in literature, e.g. [33], by comparing measured loss of light yield with simulated result of radiation-introduced decrease of light collection efficiency. It should be pointed out that the surface effect is not negligible in light collection simulation, and it is difficult to simulate. To reduce surface effect, test result of large samples are preferred in comparison with simulation.

By using a ray-tracing program originally used in BGO radiation damage study [35], a preliminary study done at Caltech showed that, to the first order, the measured loss of light yield can be explained by radiation introduced decrease of light attenuation length [23].

One important input for a ray-tracing program is the light attenuation length which usually is a function of wavelength. Figure 17a shows refractive index of BaF₂ crystal as a function of wavelength. The theoretical transmittance of BaF₂ crystals, assuming the crystal has infinite light attenuation length, is shown in Fig. 17b, taking into account of multiple bouncings of light between two faces. It is clear that at the UV edge (~ 200 nm), both the refractive index and the light attenuation length have a strong wavelength dependence. Note, if a measurement is done in air, result below 200 nm is usually not accurate because of the UV absorption of the air.

By using following formula, we calculate light attenuation length corresponding to a measured transmittance (T_m) for a 25 cm long BaF₂ crystal:

$$\ell = \frac{25}{\ln(T_s/T_m)} \quad (5)$$

where T_s is the theoretical transmittances with infinite light attenuation length (Fig. 17b).

Using a ray-tracing program [35], incorporating correct geometry, light attenuation length of the fast component at 220 nm (ℓ), 2.5 cm mass attenuation length of 0.662 MeV γ -ray from Cs source in BaF₂, light collection efficiency can be cal-

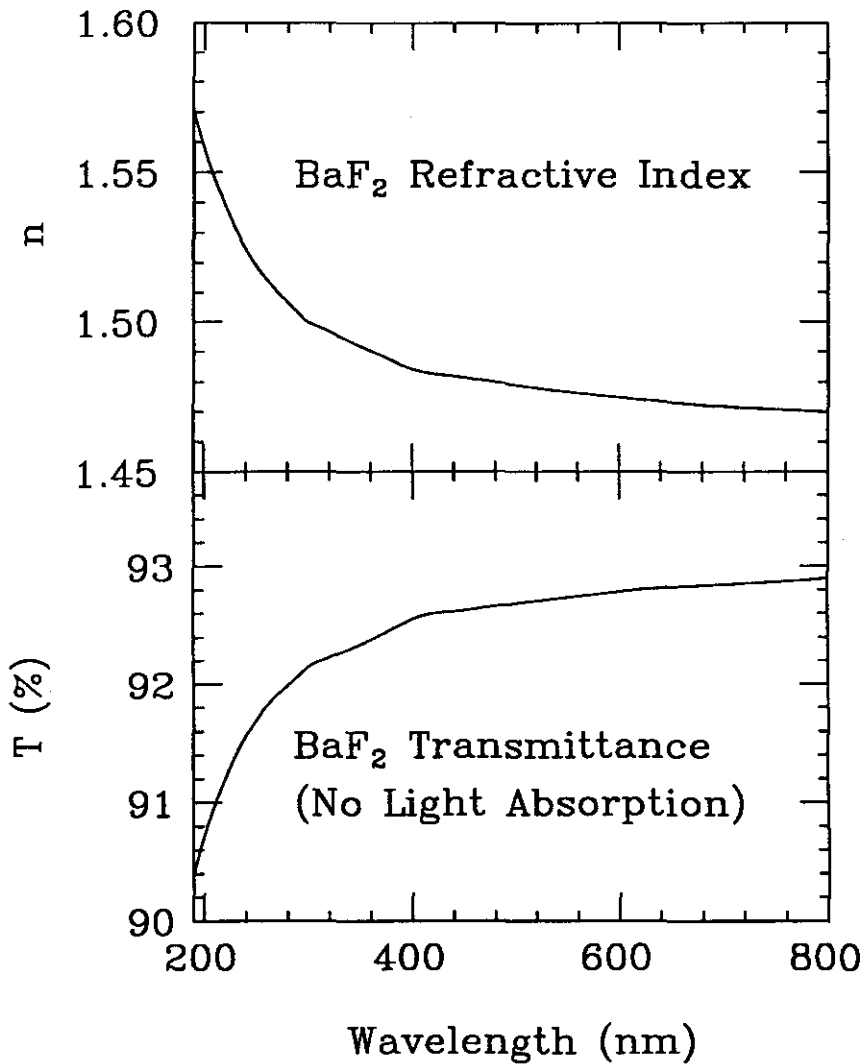


Figure 17: Refractive index (a) and theoretical transmittance (b) with infinite light attenuation length of BaF₂ crystal as functions of wavelength.

culated, and can be compared to measurements. Table 5 shows calculated light collection efficiencies (η) at 220 nm before and after irradiation, with dosage of 100, 1000 and 10,000 Rads, for two 25 cm long BaF₂ crystals from SIC/BGRI and Merck. The light collection efficiency normalized to before irradiation (η_n) and corresponding data measured at Caltech are also shown in the table.

It is clear from Table 5, that, to the first order, the measured loss of light yield can be explained by radiation introduced decrease of light attenuation length. Note, the data measured after 10,000 Rads is not accurate because of phospho-

Table 5: Comparison of Measured and Calculated Light Yield

Crystal	Dose (Rads)	T_{220nm}	ℓ (cm)	η (%)	η_n	Data
SIC/BGRI	0	84.9	354	44	1	1
	100	78.0	162	35.4	0.80	0.81
	1,000	52.1	45	16	0.36	0.32
	10,000	16.5	15	3.0	0.07	<0.20
Merck	0	75.9	137	33	1	1
	100	69.2	91	27	0.81	0.79
	1,000	49.0	40	14	0.42	0.30
	10,000	20.4	17	4.0	0.12	<0.23

rescence background.

Table 6: Transmittance and Light Attenuation Length of BaF₂ Crystals

λ (nm)	T_{surf} (%)	T_{spe0} (%)	ℓ_{spe0} (cm)	T_{spe1}	ℓ_{spe1}
200	90.6	75	130	66	79
220	91.1	80	190	70	95
550	92.7	85	290	77	135

Table 6 lists theoretical transmittance (T_{surf} , i.e. Fig. 17b), specification from BaF₂ collaboration without radiation damage requirement (T_{spe0}) and corresponding light attenuation length (ℓ_{spe0}). Assume that a 5% light uniformity may be achieved with an adequate light attenuation length (ℓ_{spe1}) at 220 nm of longer than 100 cm, Table 6 shows that a transmittance (T_{spe1}) of 10% less than original specification of BaF₂ collaboration may be allowed. Note, the light attenuation length specification of TAPS collaboration is 75 cm [36]. However, the effect on light uniformity of BaF₂ crystals with $\ell = 100$ cm must be further studied with simulation and measurements in technical proposal stage.

5.5 Understanding BaF₂ Radiation Damage (II)

The basic understanding of BaF₂ radiation damage has been significantly progressed since Shanghai Workshop, May 1991. Summarized below is basic experimental result and understanding on the mechanism of BaF₂ radiation damage, mainly achieved by chinese physicists.

The paper of Z.W. Yin *et al.* [21] shows the effect of various impurities as cations: Pb, rare earth elements (Ce, La and Eu) and transition metals (Fe and Co), and as anions: OH⁻ and oxygen. The difference in radiation resistance of different parts (top versus bottom) of BaF₂ crystals was observed. Based upon the result obtained by oxygen doped crystals, it was proposed that the radiation damage of BaF₂ was caused by O²⁻ ions (absorption in 190—250 nm) or O²⁻-F⁺ dipoles (absorption at 290 nm), where F⁺ is fluorine vacancy in BaF₂. The formation and decomposition of O²⁻-F⁺ dipoles were suggested to be responsible for the existence and disappearance (under irradiation) of the famous 290 nm absorption peak in chinese crystals.

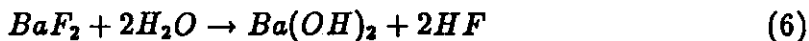
A more detailed study done by G. Chen *et al.* [24] examined the effect of trace metals of alkali, earth alkali, transition metals (Fe, Co, Ni, Mn, Cr and Cu) and rare earth elements (Ce, Pr, Nd, Eu, Tb, Dy, Ho, Tm, Yb, Y, La, Lu and Sm). While the alkali and earth alkali metals do not cause obvious damage, the transition metals do cause damage, and the rare earth elements, depending on the element, have various effects. However, the experiment was not done under controlled conditions, i.e. the impurities were not measured after crystals were grown. The experience of higher radiation resistance for Eu doped BGO [32] did not help in BaF₂ case (the same as Yin *et al.* [21]).

G. Chen *et al.* [24] also examined the effect of vacuum of the oven. Although there was no ultra high vacuum available in this experiment. The tests using ovens at 15, 53, 230 and 600 μ torr during crystal growing period show clearly that the highest vacuum, i.e. 15 μ torr, gives the best result (Fig. 13 of [24]). The study further pointed out that the vacuum at low temperature (< 600°C) is also important (Fig. 14 of [24]), which was explained by hydrolysis process of BaF₂ at low temperature.

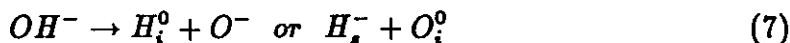
Some theoretical work was carried out by physicists from Tongji University:

L.M. Wang *et al.* and L.Y. Chen *et al.* [25]. The absorption bands of different impurities (cations or anions) were calculated by using a simple cluster model. It is interesting, however, to find that the absorption peaks of Eu doped crystal measured at 230, 347 and 370 nm (Fig. 4 of [21]) and Sm doped sample measured at 263, 334, 412, 575 nm (Fig. 12 of [24]) agree quite well with the calculation (Table 1 of [25]). This gives us some confidence on the prediction ability of this calculation. The most interesting result is the Table 2 of [25], which shows calculated broad absorption bands caused by color centers or anions.

The Tongji paper [25] further described one important experiment. They took one piece of the best SCI crystal so far made (# 12), and made several samples with it. One sample was doped with OH⁻ by heating it at 700°C under wet conditions for 12 hours. The surface hydrolysis and subsequent migration of OH⁻ ion in crystal introduced OH⁻ doping:



They then compare the absorption measurements of this sample together with two undoped control samples: one from the same crystal # 12 and another from crystal # 3 which is from an early batch. The measurements show obvious absorption band in the sample treated with OH⁻ doping. It was at 192 nm before irradiation, and was shifted to 204 nm after. They concluded that OH⁻ (absorption at 191 nm, Table 2 of [25]) was decomposed through radiolysis, and a U center (substitutional H⁻ ion, absorption at 191 nm, Table 2 of [25]) was formed:



This was further confirmed by an IR absorption at 793.75 cm⁻¹ originated from the U center, comparing with undoped sample # 3. They also found VUV absorption edge shift towards lower energy (134 → 150 nm) for OH⁻ doped crystal. The 204 nm U center absorption is also observed clearly in VUV spectrum.

An interesting comparison made by Tongji group was for oxygen doping. They tried to dope oxygen in a sample obtained from sample # 12 by heating the sample in dry oxygen at 700°C for 12 hours, i.e. under the same conditions as OH⁻ doping described above, except no water. Contrary to the sample doped with OH⁻, the result, however, showed no obvious change. They explained this observation by the difficulty in diffusing of oxygen ions into the BaF₂ crystal lattice.

Tongji group also has a different explanation of the famous 290 nm absorption. They think it is caused by OH⁻ ion. The absorption peak of free OH⁻ radical has shifted a little to red because of lattice field.

There are consensus among chinese researchers upon the radiation damage of BaF₂:

- Higher vacuum in oven improves the radiation resistance of BaF₂ crystals.
- It is not conclusive yet what is the origin of 290 nm absorption common in chinese crystals.
- While most cations are not main cause of radiation damage, some rare earth cations do produce distinguished absorption peaks. It is thus vital to remove rare earth elements in raw material.
- The OH⁻ and oxygen impurity are most fatal to the radiation resistance of BaF₂. In a matter of fact, the improved BaF₂ crystals were produced with improved processing technique which pays special attention to the removal of OH⁻ and oxygen.

In summary, chinese physicists think that they are now in correct path in understanding the radiation damage mechanism of BaF₂ crystals, and in providing solutions for the problem.

6 INTERCALIBRATION ACCURACY: b_C

Precise calibration *in situ* is vital in maintaining the high resolution of a precision detector. As shown in Table 3, the dominant contribution to the resolution of BaF₂ calorimeter at high energies is assumed to be the uncertainty of the intercalibration. It is even more so, since the radiation at the SSC would degrade the performance of the BaF₂ crystals. Assuming three sources of the irradiation: electromagnetic energy deposited in BaF₂ crystals, hadronic energy partially deposited in BaF₂ crystals and the neutron albedo [37], typical dose rate is from 50 kRads/year at $\eta = 0$ to 5 Mrads/year at the largest rapidity ($|\eta| = 2.5$) for GEM detector design.

Since the radiation damage of BaF_2 crystals saturates after initial dose and the fact of essentially *no* spontaneous annealing at room temperature, the BaF_2 crystals satisfying GEM specification (section 7), would remain to be a stable detector, although frequent and precise calibration must be provided to maintain the high resolution. In this section, we discuss two calibration schemes. One uses physics of collider — calibrate BaF_2 crystals with longitudinally penetrating minimum ionizing particles (MIP). The other uses a special calibration tool — a Radio Frequency Quadrupole accelerator (RFQ) [38].

6.1 MIP Calibration

The high flux of minimum ionizing particles produced by the collider can be used as a calibration source. A MIP passing through a BaF_2 crystal longitudinally would deposit 0.33 GeV energy in the crystal which would be readout by the crystal with a few percent resolution. With a statistics of a few hundreds tracks, the peak position or the calibration point can be determined to 0.4%. The multiplicity of charged hadrons at SSC is estimated to be large enough to provide a calibration within few working days during SSC running. Detailed study on feasibility of this calibration will be carried out in technical proposal stage.

The promise of this technique has been emphasised by recent analysis of hadronic Z^0 decays in L3, where the minimum ionizing peak signal was cleanly extracted with a simple cut on the energy in neighboring crystals, and which was observed to have a resolution $\sigma = 6\%$ (summed over all crystals). Tests with cosmic rays at UCSD, using a BaF_2 crystal pair 50 cm in length showed a resolution of 3%.

6.2 RFQ Calibration

One novel precision calibration technique for precision electromagnetic calorimeter is based on an RFQ [38]. Depending on the type of target, this calibration scheme can be run in two different modes.

The first mode uses a lithium target: the reaction ${}^7\text{Li}(p,\gamma){}^8\text{Be}$ produces a flux of 17.6 MeV photons which can be used to calibrate the thousands of electromagnetic

calorimeter cells at once, with an absolute accuracy of better than 1% in 1–2 hours. The feasibility of this calibration mode has been proven in an experimental test of a 4×5 L3 BGO crystal array [38]. An absolute calibration precision of 0.7% was achieved in the test. This low energy photon calibration, however, is not directly relevant to an SSC electromagnetic calorimeter.

The second mode [39] uses a fluoride target: the reaction $^{19}\text{F}(p,\alpha)^{16}\text{O}^*$, and the subsequent decay of the excited oxygen nucleus $^{16}\text{O}^*$, produces hundreds to thousands of 6 MeV photons per milliradian per beam pulse. These photons, functioning as a synchronised “equivalent high energy photon” of up to 30 GeV per calorimeter cell, would serve as a calibration source for SSC electromagnetic calorimeters. With a proper normalization, this technique provides a relative calibration with precision of 0.4% in a few minutes. The feasibility of this calibration mode has been proven in another experimental test with 4 BaF_2 counters and a 7×7 L3 BGO crystal array [38]. Figure 18 shows the normalized ADC distribu-

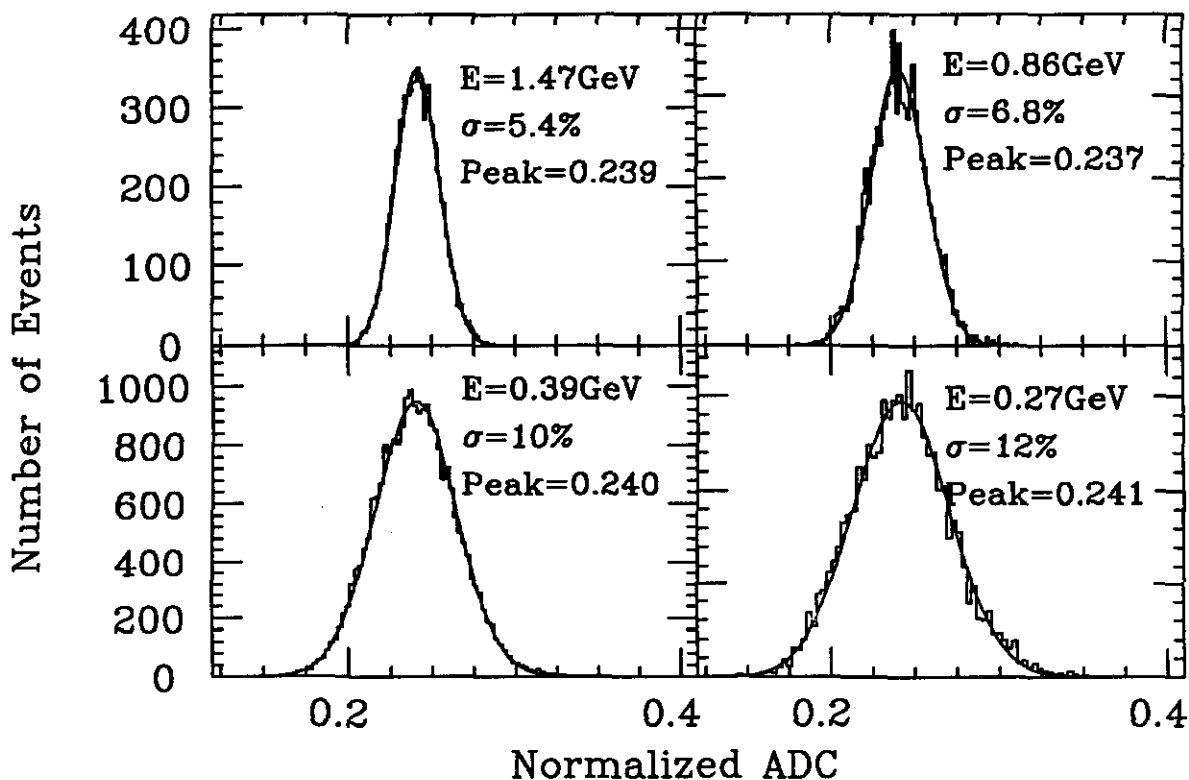


Figure 18: Normalized ADC distribution of a crystal at different energies.

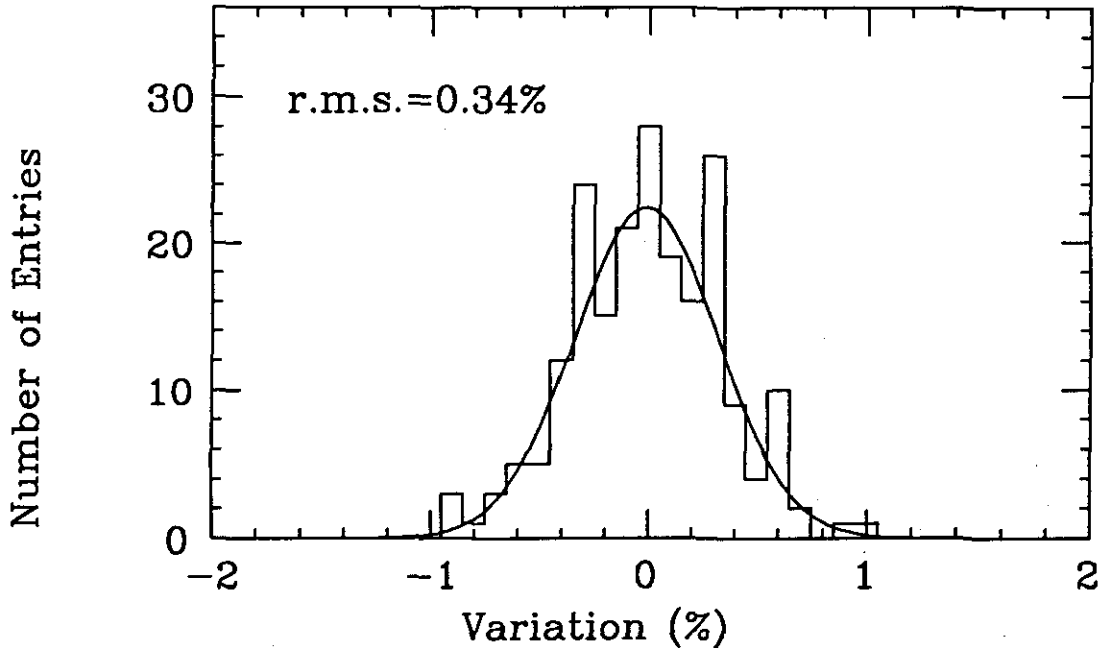


Figure 19: Variation of the normalized peak positions from BGO crystals.

tions of a crystal for runs with different beam intensities. The perfect Gaussian distribution and the correlation between the r.m.s. width and the total energy deposited in the crystal is clearly seen.

Figure 19 shows that the deviation of the peaks of 49 BGO distributions, normalized to the sum of BGO energy in the 7×7 matrix, for several runs. This distribution has a gaussian shape with a standard deviation of 0.34%. It is therefore evident that a stability of 0.4% may be achieved.

The equivalent photon energy (EPE), defined as the sum of the energies of photons from one beam pulse hitting one crystal detector, was measured at AccSys with a LiF target. Up to $2.38 \text{ GeV}/0.1 \mu\text{Coulomb}/1.6 \text{ msrad}$ was observed for a 1.92 MeV beam. There are much stronger fluorine resonances between 2.0 and 4.0 MeV [40], beyond the 1.92 MeV beam energy used in the test. By using a 3.85 MeV RFQ and a CaF_2 target, which would have no neutron production as a by-product below 4.05 MeV [40], an EPE of $30 \text{ GeV}/0.1 \mu\text{Coulomb}/1.6 \text{ msrad}$ or more is expected. Table 7 lists EPE's measured with a CaF_2 target bombarded with a proton beam from a Van de Graaff at Kellogg Lab at Caltech. The expected equivalent photon energies, calculated with an integration of the resonances [40],

are also listed in the table. It is clear that with a 3.85 MeV proton beam up to 40 GeV/1.6 msrad/0.1 μ Coulomb is achievable.

Table 7: Measured and Calculated Equivalent Photon Energy.

Proton Energy (MeV)	2.0	2.5	3.0	3.5	3.85
EPE_{meas} (GeV)	1.5	13	22	30	37
EPE_{cal} (GeV)	2.6	14	24	33	38

Two RFQ systems with exactly the specifications required for our calibration system are currently under construction at AccSys Technology, Inc. for the U.S. Navy (for a different application). One of the accelerators is expected to be available by mid-1992 for a full scale test of our technique at 3.85 MeV, using a BaF₂ prototype matrix. At least one of the accelerators could be acquired at very low cost by 1995, once the Navy's test program is completed.

7 BaF₂ SPECIFICATIONS

The specifications of the BaF₂ crystals finally will be accepted for GEM BaF₂ calorimeter are summarized in this section. The dimensional tolerances, especially for a 50 cm long crystal pair, the UV transmittance and radiation resistance are the three vital requirements.

The stringent dimensional tolerances is required to achieve a thin glue joint, e.g. few tens of μ m of KE103, and thus maintain the light uniformity. Good UV light transmittance through the crystal is vital to guarantee adequate light attenuation length for a uniform light response, and thus maintain the intrinsically high resolution of the BaF₂ calorimeter. We have specified the transmittance requirement in terms of the minimum fraction of the light passing through a 25 cm long BaF₂ crystal at specified wavelengths. For simplicity, these specifications include \sim 8% loss at two interfaces between air and BaF₂.

The radiation resistance requires that after a saturated radiation dosage the BaF₂ crystals have more than 100 cm light attenuation length for the fast compo-

ment at 220 nm. We thus propose the following specifications:

- **Dimensional tolerances** are dictated by the need to mount the crystals safely in the support structure, with a minimum of dead space between the crystals:
 - from $-300\ \mu\text{m}$ to $0\ \mu\text{m}$ in the transverse dimensions (typical deviations from nominal $100\ \mu\text{m}$)
 - from $-400\ \mu\text{m}$ to $0\ \mu\text{m}$ in length
 - less than $50\ \mu\text{m}$ in planarity of all faces after coupling two 25 cm long half crystals.
- **Transparency before irradiation**, specified in terms of the minimum fraction of the light at specified wavelengths which passes through 25 cm of crystal length:
 - $\geq 75\%$ at $\lambda = 200\ \text{nm}$
 - $\geq 80\%$ at $\lambda = 220\ \text{nm}$
 - $\geq 88\%$ at $\lambda = 550\ \text{nm}$
- **Transparency after 1 MRads irradiation**, specified in terms of the minimum fraction of the light at specified wavelengths which passes through 25 cm of crystal length:
 - $\geq 66\%$ at $\lambda = 200\ \text{nm}$
 - $\geq 70\%$ at $\lambda = 220\ \text{nm}$
 - $\geq 77\%$ at $\lambda = 550\ \text{nm}$

References

- [1] L3 Collaboration, *Nucl. Instr. and Meth. A289* (1990) 35.
- [2] BaF₂ Collaboration, *A Precision BaF₂ Crystal Calorimeter for the Superconducting Supercollider*, Subsystem R&D Proposal to the SSC Laboratory, September, 1990 and September 1991.
- [3] Crystal Clear Collaboration at CERN, Spokesman P. LeCoq.

- [4] GEM Collaboration, Letter of Intent to the SSCL, November 30, 1991.
- [5] M. Lavel *et al.*, *Nucl. Instr. and Meth.* **A206** (1983) 169;
P. Schotanus *et al.*, *Nucl. Instr. and Meth.* **A259** (1987) 586; and *IEEE-NS* **34** (1987) 76.
- [6] P. Schotanus *et al.*, *Nucl. Instr. and Meth.* **A238** (1985) 564; and Kobayashi *et al.*, *Nucl. Instr. and Meth.* **A270** (1988) 106.
- [7] P. Denes, *Electromagnetic Calorimeter Readout*, GEM TN-91-06, August 1991.
- [8] P. Schotanus *et al.*, *IEEE-NS* **34** (1987) 272; and *Nucl. Instr. and Meth.* **A281** (1989) 162.
- [9] C.L. Woody *et al.*, *IEEE-NS* **36** (1989) 536.
- [10] The K-Cs-Te cathode has been implemented in R4406 triode for BaF₂ readout. The Rb-Te cathode has been implemented in R4480 PMT for BaF₂ readout. Both tubes use quartz window and are commercially available.
- [11] Hamamatsu Photonics K.K., *R4406 specification*.
- [12] S. Suzuki, talk given in *Symposium on Detector Research and Development for the SSC*, Fort Worth, Texas, October 15—18 (1990).
- [13] Hamamatsu, *Proposal to Develop a Remote Processed Proximity Focused Phototube*, June 19, 1991.
- [14] The ATT preamplifier has 1200 electron noise for an input capacitance of 10 pf. See M. Levi, in *Symposium on Detector Research and Development for the SSC*, Fort Worth, Texas, October 15—18 (1990) 3.
- [15] R.Y. Zhu, **CALT-68-1693**, in *ECFA LHC Workshop Volume III*, Aachen (1990) 411.
- [16] The nominal gain of R4406 is 4 in the Hamamatsu specification. The reason of its lower gain, compared to the gain of 12 of Hamamatsu's standard R2148 triode, is due to the processing technology used. At present, the K-Cs-Te cathode has been evaporated inside the closed triode envelope. This contaminates the dynode. The lower gain of R4406 is due to the lower efficiency of the secondary electron emission from the K-Cs-Te contaminated dynode. By using a remote transfer technology in a large vacuum tank, this contamination will be eliminated. It is therefore expected (as indicated by Hamamatsu

themselves) that R4406 triodes produced in future, under standard production conditions, will have a nominal gain of 12.

- [17] R.Y. Zhu, *Physics Requirements to the Precision of Electromagnetic Calorimeter at SSC*, GEM TN-91-06, August 1991.
- [18] M. Kobayashi *et al.* *Transmittance and Radiation-Resistivity of Optical Glues*, KEK Preprint, 1991; Also see M. Kobayashi *et al.*, KEK Preprint 90-130, October, 1990.
- [19] KE-103 glue is manufactured by Shin-etsu Chemical Co., Japan.
- [20] W. Doering *et al.*, Total Absorption Photon Spectrometer (TAPS) Collaboration Report No. 3, March, 1988.
- [21] Z.W. Yin *et al.*, *On the Radiation Damage of Barium Fluoride Crystals*, talk given in Shanghai BaF₂ Workshop, Shanghai, May 1991.
- [22] C. Woody, *A Report on Radiation Damage in Barium Fluoride to the GEM Collaboration*, presented in GEM BaF₂ Panel meeting, December 4th (1991).
- [23] R.Y. Zhu, *On Radiation Damage of BaF₂*, presented in GEM BaF₂ Panel meeting, December 4th (1991).
- [24] G. Chen *et al.*, *Radiation Damage of Barium Fluoride Scintillator*, talk given in GEM BaF₂ Panel meeting, Beijing, December 1991.
- [25] L.M. Wang *et al.*, *The Optical and Radiation Damage Properties of Barium Fluoride Crystals*, talk presented in Shanghai BaF₂ Workshop, Shanghai, May 1991.
L.Y. Chen *et al.*, *The Radiation Damage of BaF₂ Crystals*, talk prepared for GEM BaF₂ Panel meeting, Shanghai, December 1991.
- [26] J. Zhang *et al.*, *Production of 35 cm Long BaF₂ Crystals*, talk given in GEM BaF₂ Panel meeting, Beijing, December 1991.
- [27] See for example, P. LeCoq *et al.*, in *ECFA LHC Workshop*, Aachen, October, 1990.
- [28] S. Majewski and D. Anderson *et al.*, *Nucl. Instr. and Meth.* A241 (1985) 76; A. J. Caffrey *et al.*, *IEEE Trans. Nucl. Sci.* NS-33 (1986) 230; and S. Majewski *et al.*, *Nucl. Instr. and Meth.* A260 (1987) 373.
- [29] P. Schotanus *et al.*, *Nucl. Instr. and Meth.* A272 (1987) 917 and *Technical Univ. at Delft Preprint 88-1*.

- [30] Z. Wei *et al.*, *Nucl. Instr. and Meth.* **B61** (1991) 61.
- [31] J.T. He *et al.*, *On Radiation Damage of Barium Fluoride Crystals*, talk given in Shanghai BaF₂ Workshop, Shanghai, May 1991.
- [32] R.Y. Zhu *et al.*, *Nucl. Instr. and Meth.* **A302** (1991) 69;
Z. Wei *et al.*, *Nucl. Instr. and Meth.* **A297** (1990) 163;
T.Q. Zhou *et al.*, *Nucl. Instr. and Meth.* **A258** (1987) 464.
- [33] C. Woody *et al.*, *Radiation Damage of Barium Fluoride Crystals*, paper presented at IEEE Nuclear Science Symposium, Santa Fe, New Mexico, Nov 5—8, 1991.
- [34] Z. Wei *et al.*, *A Study on Radiation Damage of Barium Fluoride Crystals*, to be submitted to *Nucl. Instr. and Meth.*.
- [35] The ray-tracing program was originally written L.Gatingnon and D. de Lang of University of Nijmegen, and was substantially modified by R.Y. Zhu in 1986.
- [36] R. Novotny, *Performance of BaF₂ -Crystals*, (TAPS) Collaboration Report No. 10, February, 1990, and No 10/1, October 1990.
- [37] D.E. Groom, *Radiation Levels in the SSC Interaction Regions*, Task Force Report, June, 1988.
- [38] R.Y. Zhu, *Nucl. Instr. and Meth.* **A306** (1991) 145;
H. Ma *et al.*, *Nucl. Instr. and Meth.* **A274** (1989) 113; and *Nucl. Instr. and Meth.* **A281** (1989) 469.
- [39] R. Hamm *et al.*, *An SSC Electromagnetic Calorimeter Calibration Source*, Final SBIR Project Report to the Dept. of Energy, AccSys Technology Inc., Pleasanton, California, August, 1991.
- [40] F. Ajzenberg-Selove, *Nucl. Phys.* **A475** (1987) 1; and H. B. Willard *et al.* *Phys. Rev.* **85** (1952) 849.